AN OBSERVATIONAL AND NUMERICAL CASE STUDY OF THE NORTHERLY LOW-LEVEL JET OVER THE GREAT PLAINS OF THE UNITED STATES

By

Jovanka Nikolic

A THESIS

Submitted to
Michigan State University
in partial fulfillment of the requirements
for the degree of

MASTER OF SCIENCE

Geography

2012

ABSTRACT

AN OBSERVATIONAL AND NUMERICAL CASE STUDY OF THE NORTHERLY LOW-LEVEL JET OVER THE GREAT PLAINS OF THE UNITED STATES

By

Jovanka Nikolic

Low-level jets (LLJs), streams of fast-moving air in the lower atmosphere, have a strong impact on the weather and climate of the Great Plains of the United States. Southerly LLJs are known to play an important role in transporting moisture and heat from the Gulf of Mexico northward and are primarily responsible for the summertime nocturnal convection in the Great Plains region, whereas Northerly LLJs have been linked to blizzards and large spread of wildfires. While numerous studies have examined the properties and forcing mechanisms of southerly LLJs, little is known about the formation and characteristics of the NLLJs.

In this study, we apply the Weather Research and Forecast (WRF) model to simulate two historical cases of a well-developed NLLJ. The purpose is to improve the understanding of the structure and evolution of NLLJ and the large-scale and local atmospheric environments in which they form. The WRF model is configured with multiple nested grids and is initialized using the North American Regional Reanalysis (NARR). The simulation results are compared with both surface and upper-air observations. Simulations were performed with different model physical parameterizations and process analyses are performed to help identify important factors important for the formation of the NLLJs.

To my loving husband, sister, and parents who gave me the courage, confidence, and strength I needed to accomplish my goal

ACKNOWLEDGMENTS

I would like to thank my advisor Dr. Shiyuan Zhong for her advices, teaching, and review of this thesis, Dr. Julie Winkler, Dr. Claudia Walters, and Dr. Alan Srock for their constructive comments on the thesis, and Dr. Joseph Charney and Mr. Xindi Bian for their assistance with WRF. I would also like to thank USDA Forest Service Northern Research Station for providing computing resources.

Finally I would like to thank my husband Mihailo, my family and friends, for supporting me at every step of my way. Their encouragement always "gives me the wings to chase my dreams".

TABLE OF CONTENTS

LIST OF TABLES	vii
LIST OF FIGURES	viii
CHAPTER I Introduction	1
CHAPTER II Literature ReviewObservational studies	
Numerical studies	
CHAPTER III Objectives of the Current Study	19
CHAPTER IV Data and Methodology	20
Case Selection	20
CHAPTER V	
Results	
April case	
Synoptic analysis	
WRF simulation	
September caseSynoptic analysis	
WRF simulation	
CHAPTER VI	
Discussion	60

CHAPTER VII

Summary and Conclusion.	65
APPENDIX	68
REFERENCES	73

LIST OF TABLES

Table 1.	List of physical parameterization schemes used by each model run	.26

LIST OF FIGURES

Figure 1. Surface weather charts for a) September 19 th , 1991 at 7 a.m. local time, and b) April 29 th , 1991 at 7 a.m. local time. "For interpretation of the references to color in this and all other figures, the reader is referred to the electronic version of this thesis (or dissertation)."
Figure 2. Rawinsonde observations of wind speed and direction taken at a) 12 UTC, 19 September, 1991 from the OUN station, and b) at 12 UTC, 29 April, 1991 from the LBF station
Figure 3. Distributions of the NARR-derived mean sea-level pressure and temperature (top panel), 800 hPa geopotential height, temperature and wind speed (middle panel), and 250 hPa geopotential height and winds (bottom panel) for April 28-30, 1991
Figure 4. Vertical profiles of wind speed simulated by WRF using different physical parameterizations taken from the innermost grid from the model grid point closest to the OUN station at 12 UTC, September 19, 1991 (up), and from the model grid point closest to the LBF station at 12 UTC, April 29, 1991 (bottom)
Figure 5. Distriution of the WRF-simulated mean sea-level pressure and 2 m temperature, 800 hPa geopotential height and temperature, 250 hPa geopotential height and wind speed for 12 UTC, April 29, 1991
Figure 6. Modeled, observed and NARR vertical wind speed profiles at 12 UTC, April 29, 1991 at the LBF station
Figure 7. Cross sections of the simulated wind speed (shading) and contours of potential temperature (a) and turbulent kinetic energy (b) in the plane perpendicular to the jet core on at 12 and 18 UTC on September 19, 1991near the LBF station
Figure 8. Distribution potential temperature (contours), specific humidity (shading) and wind vectors for 800 hPa pressure level between 00 UTC, April 29 and 00 UTC, April 30, 1991

Figure 9. Vertical profiles of simulated wind speed, specific humidity and potential temperature at LBF station on 29 April, 1991
Figure 10.Distribution of the NARR-derived mean sea-level pressure and temperature (top panel), 900 hPa geopotential height, temperature and wind speed (middle panel), and 250 hPa geopotential height and wind speed (bottom panel) for September 19-20, 1991
Figure 11. Distribution of WRF-simulated the mean sea-level pressure and 2 m temperature, 900 hPa geopotential height and temperature, 250 hPa geopotential height and wind speed for 12 UTC on September 19, 1991
Figure 12. Modeled, observed and NARR vertical wind speed profiles at 12 UTC, 19 September 1991 at the OUN station
Figure 13. Same as Figure 7, but for September 19, 1991 with the center of the cross sections near the OUN station
Figure 14. Distributions of 875 hPa level potential temperature (contours), specific humidity (shading) and wind vectors for the time period between 00 UTC, 19 September and 06 UTC, 20 September, 1991
Figure 15. Vertical profiles of simulated wind speed, specific humidity and potential temperature at OUN station on 19 September, 1991
Figure 16. Geostrophic (blue) and ageostrophic (red) wind at 800 hPa surface on April 29, at 12 UTC (upper), and at 900 hPa surface on September 19, at 12 UTC (bottom)

CHAPTER I

Introduction

Low-level jet (LLJ) is an atmospheric phenomenon observed at every continent, and it is defined as a wind maximum in the lower troposphere. LLJ is usually related to transport of moist air from one region to another, so it is commonly associated with heavy precipitations and thunderstorms.

Some authors divide LLJ into several jet types, depending on forcing mechanisms. Sladkovic and Kanter (1976) recognize four LLJ types: orographic, thermal, nocturnal, and synoptic scale jet. Orographic LLJ type is the jet that forms because of orographic lifting or terrain channeling. Some examples of this jet type are the South Americas' jet in Argentina and the mistral in southern France. Thermal LLJ is the jet type forced by temperature gradient over some areas. Some examples of this jet type are valley wind and sea-land breeze. Nocturnal LLJ is the most commonly studied jet type. This jet is observed during nighttime and the primary mechanism for its formation is the development of surface-based stable layer. The jet is located at the top of the stable layer and the maximum wind speeds are usually greater than the geostrophic wind aloft. Synoptic-scale LLJ is the jet type with most diverse formation mechanisms. The type of jet can be initiated by cyclogenesis and passage of fronts or similar synoptic-scale features. Compare to other types, this type of LLJ usually has stronger maximum wind speed. The jet nose is usually located at the top of temperature inversion, and the height of the nose changes over time with the height of the inversion. Horizontal extension of this jet type can be several hundred kilometers.

LLJ is observed at all continents, but one of most studied LLJs is the southerly LLJ (SLLJ) over the Great Plains of the United States. A climatology of the Great Plains SLLJ was first developed by Bonner (1968) using 2-year rawinsonde data. He reported that SLLJs are most commonly observed in early morning soundings and they are most frequent in summer and least in winter. The highest frequency of SLLJ is observed in Oklahoma and Kansans over the southern Great Plains. Whiteman et al. (1997) used enhanced rawinsonde observations available eight times per day, for two years, and found that LLJs are located at much lower heights that had been reported previously (300-600 m above the ground). Walter et al. (2008) developed 40-year jet climatology. They found that SLLJs are most frequent in summer over the Plains and along the western Gulf Coast, while during spring and autumn jets occur most often over the areas from the central Gulf Coast northward to the Great Lakes. Also, summertime jets are usually weaker southerly jets, while stronger SLLJs can occur year round.

The physical mechanisms responsible for the development, evolution, maintenance and dissipation of the Great Plains LLJ was investigated by Zhong et al. (1996) using a mesoscale numerical model. They found that the primary governing mechanisms for the formation of the SLLJ are frictional decoupling and inertial turning by the Coriolis force.

Much less work has been conducted on northerly LLJs (NLLJ). This type of LLJs occurs year around, but is more frequent in the cold season. Whiteman et al. (2008) in their climatological study identified NLLJs. According to their findings, NLLJs usually occur during daytime, and the height of the wind maximum is more variable for northerly jets compared to southerly jets. Walters and Winkler (personal communication) in their study identified 16 different northerly LLJ types. A NLLJ could be located next to surface cyclone or anticyclone.

Jets located northwest or west of the cyclone center are usually located closer to the cyclone center. Jets associated with a surface anticyclone (with diffluent airflow above the anticyclone) have high wind speeds to the east or southeast of the anticyclone center. As noted by Carlson (1980) in his study, and confirmed by Walters and Winkler (personal communication), northerly jet events related to cyclonic flow can be found in branch of a 'drystream'.

Little is known about the structure of NLLJs and the physical mechanisms responsible for their development, maintaining and dissipation. Similarly, no studies, to our knowledge, have carefully examined the ability of mesoscale atmospheric models in simulating NLLJ events. Although previous climatological studies have suggested that NLLJs are less frequent than SLLJs over the Great Plains, these NLLJs could have large impacts on many practical applications such as aviation, fire weather, wind energy, and air pollution transport and dispersion. Accurate forecast of the formation and evolution of NLLJs over the Great Plains is important for these applications.

In this study, the Weather Research and Forecast Model (WRF) is used to simulated two NLLJ episodes. The specific objectives of the study are: 1) to evaluate the ability of the state-of-science regional atmospheric model in simulating the structure and evolution of the NLLJs; 2) to explore the sensitivity of simulations to model physical parameterizations; and 3) to provide detailed depiction of the NLLJ structure and the atmospheric environments in which they develop.

CHAPTER II

Literature Review

Since LLJ has been detected in all continents, numerous studies have been conducted all over the world in order to better explain this interesting and important atmospheric phenomenon. In the following, we provide a review of LLJ studies.

Observational studies

An early observational study conducted by Sladkovic and Kanter (1976) used 1500 vertical-profile measurements obtained by balloon flights in order to investigate different types of LLJ in Europe. They recognized four different jet types: orographic LLJ, thermal LLJ, nocturnal LLJ, and synoptic scale LLJ. Maximum wind speeds varied with the jet type, from 10 m s⁻¹ for nocturnal jets to 30 m s⁻¹ for synoptically driven jets. Also, the height of the jet varies with the jet type, from 100-200 m above ground for thermal LLJ to 700-1200 m for synoptic-scale LLJ. They pointed out that proper forecasting of synoptic-scale LLJ is of highest practical importance, especially for needs of aviation services.

Using the Koorin expedition data, a collection of 30-day hourly wind and 3-hour temperature measurements up to 3 km, Brook (1985) studied LLJ observed at Daly Waters, Australia. The study found that the jet changes over a diurnal cycle, with strongest wind speeds observed in the early morning and jet disappearance later in the day. The jet is located at the top of a surface inversion. Using a simple model where the forcing is produced by a variation in eddy viscosity term, the study identified inertial oscillation as the primary mechanism for jet formation, and sloping terrain as secondary cause.

One of the main concerns in urban areas located near heavy industries is concentration of air pollutants and dispersion of emitted substances that can be harmful to human health. Jury et al. (1989) investigated winter boundary layer in the Johannesburg region in an attempt to understand the dispersion capabilities of the region. They used horizontal and vertical wind data, and horizontal and vertical component deviations. Their results indicate that LLJs that develop over the region are responsible for dispersion. They found that there is no single mechanism responsible for the jet formation. Wind maximum is located at the top of the inversion, and the drop in the value of drag coefficient is responsible for the formation of higher wind speeds. Various mechanisms suggested in the literature were used to explain the LLJ in this region. The inertial oscillation, which had been considered to be the primary forcing for LLJs in many other places, was not supported by the data in their cases. Instead, the LLJ was thought to be a result of thermal gradient.

A low-level northwesterly wind known as Shamal, often blow over Iraq and Persian Gulf states between May and July when the skies are mostly clear over the region. During daytime, heating of the lower layers of the atmosphere is intense and the layer is well mixed, while winds above the mixed layer are almost geostrophic. At night, on the other hand, boundary layer is very stable due to strong radiational cooling, and a strong surface temperature inversion develops. Winds over this surface inversion become supergeostrophic which, when combined with weaker surface winds due to friction, lead to the formation of a jet profile. Membery (1983) showed that the maximum wind speed, which is around 10 ms⁻¹ at 900 m above ground, is usually reached four and a half hour after sunset and at latitude 26 °N.

Strong cross-equatorial jet is responsible for transport of moisture in this region. This low-level cross-equatorial jet stream is one of the main features over eastern Africa and the West

Indian Ocean during the monsoon period. The jets with maximum wind speeds of 25 – 50 ms⁻¹, at the height of 1-1.5 km, extend from April to October, with maximum strength observed in July. The jet flows from Mauritius and Madagascar, Kenya and Ethiopia, over the Arabian Sea to western coast of India. According to Findlater (1969), maximum cross-equatorial mass transport is located between 38 °E and 55 °E and below 3000 m. The maximum and minimum of this cross-equatorial flow are associated with the maximum and minimum amount of rainfall over west coast of India. The intraseasonal oscillation in LLJ characteristics controls moisture distribution over India.

A study on LLJ in Llanos was performed by LaBar (2006) as part of National Weather Center Research Experiences for Undergraduates final project. In this study, pilot balloon soundings taken at 1200 UTC at San Fernando de Apure, Venezuela, cloud-top temperature frequency composites based on high-resolution infrared satellite images, and NCEP North American Regional Reanalysis (NARR, Mesinger et al. 2006) zonal and meridional wind fields for the period between March 2001 to May 2005 are used to understand the characteristics of low-level winds over the Llanosgrass plain. In order to locate height and time of the year where strongest wind speeds above the Llanos occur, plots of the pilot balloon observations and the interannual variation of zonal wind speeds with height for both wet (May-September) and dry (November-March) seasons are generated. Similar wind plots are made from the NARR data for the period between 2001 and 2004. Analysis of these plots over the Llanos showed wind speed maxima at approximately 1000 m above the ground from late January to March, with a maximum of 15.5 ms⁻¹ from the east. Zonal wind speed plots for San Fernando shows the wind speed maximums of 14 to 15 ms⁻¹, at about 650 m. For both regions, winds are weakest in July

and August. A comparison of plots generated from the pilot observations and from the NARR data shows that the NARR data is in good agreement with actual observations, and can be used for studies related to Venezuelan LLJ.

To understand the mechanisms associated with the formation and development of the SLLJs, many studies have relied on direct observations. Pitchford and London (1962) examined summer observations from 21 stations around Omaha for three summers. They also looked at percent of reported thunderstorms for that period over night (from 00 to 06 local time), with respect to mean wind charts. They found that the presence of a LLJ is closely related to the occurrence of nocturnal thunderstorms in that region. When the jet axis is orientated north-south or north-southwest, the thunderstorm frequency is high.

The University of Wyoming Beechcraft Super King Air instrumented research aircraft was used during July 1983 to observe the height of the isobaric surface, as well as vertical profile of LLJs (Parish et al. 1988). This study confirmed that diabatic heating and cooling of the sloping terrain produce a horizontal pressure gradient that inducts the forming of a LLJ. However, in a different study by Frisch et al. (1992) where Doppler radar was used to observe one typical boundary-layer inducted LLJ, it was shown that the pressure gradient change was not the main contributor to the jet's development.

Kapela et al. (1995) analyzed post cold frontal wind events that happened on January 10, 1990 over the Northern Plains, and identified several atmospheric factors that contribute to high winds. They suggested that these LLJs are aligned with an upper-level jet and that strength of the upper jet is associated with the LLJ maximum speed, with stronger upper jet causing higher NLLJ maximum speeds. Also, these NLLJs are associated with a strong subsidence.

LLJs were also observed on the east coast of Southern Africa. The vertical motions are limited by existence of inversion and terrain configuration, so the flow is parallel to the Drakensburg mountain range that is starched along the coast (Kelbe 1988). In another study, Jury et al. (1988) used sounder data close to Cape Town, with vertical resolution of 50 m up to 1000 m, and temporal resolution 15 minutes to study low-level winds. In addition to the sounding data, they also used 10 m wind data, surface station data, temperature profile measurements up to 100 m, and measurements obtained by aircraft flights The period of the study was from mid-November 1984 to February 1985. Although the main goal of the study is to develop wind climatology, the occurrence of nighttime LLJ was documented. Wind is topographically channeled to follow the west coast. During nighttime, the southeasterly trade wind maximum at the lee side of the costal mountain range was detected. Analysis of the temperature, moisture and wind speed fields showed nighttime temperature inversion between 1000 and 971 hPa, and upper-level inversion located around 876 hPa, with unstable layer located between the two inversions. Wind speed maximum of 16 m s⁻¹ was observed within this unstable layer, where the upper inversion helps the acceleration of the jet over Table Mountain. The jet appears after the daytime acceleration of the southeasterly wind due to existence of horizontal temperature gradient, and over night, because of low-level inversion, wind is able to accelerate and the jet forms at approximately 300 m above the ground and strengthen northward.

Sijikumar (2003) performed climatological analysis of summer monsoon rainfalls along the west coast of India and the relation to low-level flows using NCEP/NCAR reanalysis daily wind data, NOAA longwave radiation data, and Indian Summer Monsoon Rainfall (ISMR) data. The results show large inter-annual variability over the 30-year study period, with some years (refers to as dry years) having much less than average rainfall amounts, while other years (refers

to as wet years) having much higher than average rainfall amounts. The data analyses confirmed that cross-equatorial flow and winds over Arabic sea are stronger during wet years, while during so-called dry years, winds are weaker. So, seasonal and annual variability of the monsoon activity is related to LLJ variability. The rainfall amounts and convection over the west cost of India are closely investigated by the MM5 model. The main finding from model simulations is that they are closely related to the cyclonic shear in the boundary layer associated with the LLJ. On the other hand, LLJ maximum wind speed is preserved or increased by the atmospheric heating from convection over the Bay of Bengal.

Several studies have developed the LLJ climatology over the Great Plains of the United States. The first LLJ climatology was reported by Bonner (1968) using 2-year, twice daily rawinsonde data. He found that LLJs are most frequent over the Great Plains and that LLJs appeared in early morning soundings more often than in afternoon soundings. He noted that the jet wind speeds and the heights of the wind maxima varied greatly from case to case and that the heights of the wind maxima were not strongly correlated with the heights of nocturnal surface inversions.

Mitchell et al. (1995) used hourly observations from the Wind Profiler Demonstration Network during two-year warm seasons to document the average strength, frequency of occurrence, and temporal-spatial variability of LLJ over the Great Plains. They also evaluated the synoptic patterns for LLJ occurrence. The LLJ was primarily out of the south or the southwest with maximum activity in late August and September. It typically occurred between 0600 and 0900 UTC, with duration of about 4 hours. The synoptic environment with forcing mechanisms related to diurnal boundary-layer development acted together to produce strong LLJs.

Another climatological study of the Great Plains LLJ was conducted by Whiteman et al. (1997) that used rawinsonde data obtained up to eight times per day with enhanced vertical resolution over a two-year period at a site in north-central Oklahoma near the center of the maximum LLJ occurrence. This study showed that jets are stronger than previously reported and the heights of maximum wind speed are closer to the ground. The frequencyof occurrence of LLJs is found to be almost the same for the warm and the cold seasons. The height of the jet maximum occurs most frequently in the 300–600 m height range, with a peak between 300 and 400 m. The study found that some of observed LLJs have the winds at the level of the jet maximum from the north (so called northerly LLJs). Southerly LLJs have a much higher frequency at nighttime than during daytime and undergo a distinct diurnal clockwise turning in wind direction at the height of maximum speed. In the cold season there is decreased frequency of the southerly jets. Unlike previous studies, they found that the highest jet wind speed category has a much higher frequency than expected from earlier climatologies and the mean height of LLJ wind speed maximum is much lower than expressed in earlier climatologies.

A forty-year (1961–2000) climatology of southerly and northerly LLJs (LLJs) based on twice daily rawinsonde observations from 36 stations in the central United States was presented by Walters et al. (2008). The jet characteristics were summarized by direction, season, time of day (00 UTC and 12 UTC), and intensity category. During summer and fall the frequency maximum shifts northward to northern Texas, Oklahoma, and southern Kansas. Southerly LLJs are most frequent in summer in an area from the northern to the southern Plains and along the western Gulf Coast, while from the central Gulf Coast northward to the Great Lakes, southerly jets occur most often in spring and autumn. Weak southerly jets are more frequent in the warm season and strong jets don't have uniform distribution over the seasons. Jets with less wind speed

are more frequent along the Gulf of Mexico coastline in summer. Both southerly and northerly LLJs are more frequent in the morning than in the evening. The direction of southerly jets tends to rotate from a more southerly direction at 00 UTC to a more southwesterly direction at 12 UTC, especially in summer. Different forcing mechanisms are found to be responsible for LLJ formation over central US.

Although southerly LLJs have been frequently studied (Pitchford and London 1962; Parish et al. 1988; McCorcle 1988; Fast et al. 1990; Mitchell et al. 1995; Zhong et al. 1996), less work has been conducted on northerly LLJs. This type of LLJs occurs year around, but is more frequent in the cold season.

The two LLJ climatological studies mentioned above (Whiteman et al. 1997 and Walters et al. 2008) included analysis of NLLJs. Whitman et al. (1997) found a significant number of northerly LLJs that have the winds at the level of the jet maximum blowing from the north. In contrast to southerly LLJ that has a strong diurnal variation in the frequency with a pronounced nocturnal maximum, northerly jets have a weak diurnal variation in their frequency of occurrence, with the highest occurrence during daytime. Also, the height of the wind maximum is more variable for northerly jets compared to southerly jets. The northerly jets show small and irregular diurnal wind direction shifts and are usually associated with high pressure, low specific humidity, and low temperature at the surface. They are also frequently found below elevated temperature inversions. An inspection of synoptic charts shows that the northerly LLJs frequently occur behind cold fronts that move southward. The jets occur in the cold, slightly stable air behind the front, and the depth of this cold air and the height of the jet maximum increase with distance behind the front.

In Walters et al. (2008)'s study, it was found that the northerly LLJs have significant

differences in characteristics from the classical southerly LLJs. These jets are usually associated with traveling synoptic-scale weather systems. The northerly jets occur most often in the Northern Plains, although secondary maxima are seen in the region of the Great Lakes in spring and along the western Gulf Coast in autumn. They displayed little systematic variation in the wind direction during the observation time. Whether weak or strong, northerly jets have low frequency in summer and high in autumn and winter. Little research has been conducted on possible boundary-layer forcing of northerly LLJs.

A more recent study examined in great detail two multi-day NLLJ episodes, one with primarily cyclonically-curved jets and the other with primarily anticyclonically-curved jets (Walters et al. personal communication). A local wind speed maximum (also called a 'jet profile signature' (JSP) or a 'jet nose') was identified in the vertical direction from twice-daily rawinsonde observations in central North America, and the two-dimensional airflow of NLLJ (the jet event) was then assessed from streamline and wind speed analyses for the isentropic surface that intersected each JPS. Walters et al. (2008) identified airflow patterns with approximately 52% of the jet events observed with broadly anticyclonic airflow, 37% with cyclonic airflow, and 11% with 'neutral' airflow. All airflows were classified in 16 different type groups. A NLLJ northwest or west of the cyclone center has cyclonic airflow and could originate from different directions. Such jets are closer to the cyclone center and have confluent cyclonic airflow and non-diffluent cyclonic airflow at some distance of the center. NLLJs events observed east of a surface anticyclone originate in the lower or mid troposphere, with diffluent airflow above the anticyclone and the strongest wind speeds expected to the east or southeast of the anticyclone center. Neutral jet events have little curvature airflow with the transition between the anticyclone and a cyclone to the east. The case studies covering the period from 1 January to 31

December 1991 (Walter et al. 2008). For each case study, plots of mean sea-level pressure, 500 hPa geopotentialheight, and 200 or 300 hPa (depending on the season) streamlines and wind speed were used to investigate the synoptic environment in which the jet events occurred. By result analysis, Walters et al. (2008) concluded that a Cyc-C-N/NW (Cyclonic, confluent, originates from the north/northwest) jet event observed early in the time sequence transform to dominantly northeasterly airflow (Cyc-CE/NE (Cyclonic, confluent, originates from the east/northeast), Cyc-ND-NE (Cyclonic, non-diffluent, originates from the northeast), and Neu-E (Neutral airflow originating from the east)) by time. Analyzing the NLLJ related to anticyclones on a surface, the jet events at the individual observation times were classified as Ant-D-ctr (Anticyclonic, diffluent, originates from an obvious diffluent center), with the center located somewhat west of a surface anticyclone. This study confirmed the idealized schema of the relationship of NLLJ jet events to the centers of surface anticyclones and cyclones.

Numerical studies

One of the main mesoscale features in southern France is heavy precipitations related to organized convective systems. Many researchers examined this weather characteristic (Senesi et al. 1996; Buzzi and Foschini 1999; Lebeaupin et al. 2006;), and they all concluded that the LLJs over the region are the main element responsible for the formation of these convective systems. Senesi et al. (1996), in their analysis of heavy flash floods in the Vaison-La_Romaine city of southern France, found that strong LLJs, with wind speeds as high as 45 ms⁻¹, were feeding the system with the moist air from the Mediterranean Sea, which in combination with slow-moving cold front, increased the possibility for the development of deep and strong convection and

heavy precipitation. In their analysis of numerical model outputs, they concluded that operational forecast underestimated the jet position, shifting and strength.

Buzzi and Foschini (1999) studied heavy precipitations over the southern Alpine region. By using the mesoscale model BOLAM3 they found that strong low-level flow from the south, in front of the cold front from the western Mediterranean, is the main feature that supplies the region with the warm and moist air, initiating formation of organized convective systems.

Lebeaupin et al. (2006) looked at heavy fall precipitations over the southern France region, and they also found that moisture that feeds almost stationary convective system and extends its life time is provided by a LLJ that brings moisture from the Mediterranean Sea. They used two different convective parameterization schemes available in the MESO-NH research model, and found complex relationship between LLJ and latent heat fluxes for both parameterization schemes. In the case the southwesterly diffluent flow over southern France on early September (Gard case), latent heat decreases with strong LLJ, and as a result, precipitation is less intensive. On the other hand, in a case associated with a southerly flow from North Africa to southern France (or November case), strong LLJ has little influence on total precipitation. In the case where a slow moving frontal system is situated over southern France, LLJ has no influence on precipitation.

Low-level wind maxima, called Mistral are reported over the Gulf of Lions. This LLJ is a result of channeled cold air accelerating over the Rhone Valley due to the surrounding Alps and Massif Central mountains. Lebeaupin and Dobrinski (2009) examined the relationship between LLJ over the Rhone Valley and the boundary layer over the sea. They investigated how sensitive the coupled slab ocean model and Weather Research and Forecasting model (WRF) is to different physical configurations. Using WRF simulations, they found that the peak wind speed

of the LLJ appears at the same time as a maximum energy transfer between sea and planet boundary layer (PBL). Also, they found that sea boundary layer is the thickest at the time of maximum LLJ. The influence of LLJ on the structure of the sea boundary layer is found to vary with the time of the year and temperature contrast between the sea and the land with large influence in the fall season and weak influence in the spring season. Their study concluded that depending on the strength of LLJ, high resolution and two-way coupled model is needed in order to accurately predict the ocean state. In a similar study, Drobinski et al. (2005) looked at three dimensional (3D) characteristics of the Mistral over the Rhone Valley Delta using a combination of high-resolution, non-hydrostatic Penn State-National Center for Atmospheric Research (NCAR) mesoscalemodel (MM5) and radiosonde and surface data as well as Doppler lidar wind data. They found that PBL height is lower under Mistral than continental PBL height. Their results confirmed that the jet is formed due to wind acceleration between two mountain ranges (Alps and Massif Central), and that acceleration occurs until hydraulic jump appears. After the hydraulic jump, wind speed decreases, and wakes form at the mountain tops.

The East China Plain (also known as Huang-Huai-Hai Plain) is similar to the Great Plains of the United States in terms of topography and importance for the food production. In their study, Zhong and Wang (2000) have examined the relationship between LLJs developed over the Huang-Huai-Hai Plain and the inversion over the Plain over agro-forest canopy using a simple model and radiosonde observations for a 4-day period. They show that temperature inversion forms and deepens over night, and a LLJ develops at the top of that inversion, and then disappears after sunrise. Different inversion intensities are employed in the model to investigate how it would affect both the intensity and the height of the jet and the results show that the more intense inversions will result in stronger LLJs. An examination of the effects of geostrophic

forcing show that geostrophic wind speeds between 6 and 10 ms⁻¹ at the model top is favorable for the development of the LLJ. A closer look at the roughness length and LLJ relationship revealed that LLJ height will increase with increased roughness lengths.

Vernekar et al. (2003) compared Eta Model simulation of summer climate for 1983, '85, '87 and 1991 with NCEP global reanalysis for Central and South America region. They found that Eta Model simulations are more realistic than the same features in the reanalysis data. The Eta is able to predict the LLJ east of Andes, its horizontal and vertical structure. The jet favorites development of convection and conditions that brings precipitations over the region, with maximum precipitations over night in the region influenced by the jet. Regions out of the jet influence have precipitation maximum in the afternoon. Also, stronger jets are observed during El Nino years than during La Nina years.

Saulo et al. (2000) looked at models' capability to simulate LLJ characteristics. They employed a regional model with 38 vertical levels and 40 km horizontal grid resolution, and compared rawinsonde observations with the model runs for 12 different cases to verify the model. The model simulations showed that South America low-level jet (SALLJ) occurs almost every day, with less occurrence days in February. Data discovered another LLJ over the Atlantic Ocean with the stronger signal when SALLJ is weaker. The study also looked at water vapor transport, and found a maximum between 00 and 06 UTC at 900 hPa surface, with southward component up to 600 hPa. The surface acts as a sink for the atmospheric moisture, where the moisture is transported southward by a SALLJ and Atlantic anticyclone. At the higher levels, western boundary influx provides moisture.

In a more recent study, Silva et al. (2010) examined how the choice of convective schemes affects the models' capability to predict LLJ. The RegCM 3 model (Pal et al. 2007) was

run with two different convective parameterizations and the results were compared with the observations. The Emanuel scheme simulates stronger LLJ than the Grell scheme. The model underestimates LLJ frequency compared to the observations, with Emanuel scheme showing greater relative frequency of the jet than the Grell scheme.

To study the effects of soil moisture on the development of LLJs, a three-dimensional boundary-layer model developed by Paegle and McLawhorn (1983) was coupled with a soil-moisture predicting system and applied to a nocturnal jet case over the Great Plans (McCorcle 1988). The model predicted the occurrence of the Great Plains nocturnal jet, as well as the magnitude of jet wind speed. Also, the model investigated soil moisture influence on the ground pressure gradient that is responsible for development of the LLJ. The results showed a reduced buoyant slope circulation over the moist soils, and thus decreased opportunity for jet development.

A similar coupled model was used to examine the specific effects of inhomogeneous surface energy distribution at the ground on the structure of the nocturnal jet (Fast et al. 1990). Model output analysis demonstrates that the slope of the Great Plains is very significant for the summertime jet. The LLJ produced over flat terrain was weak and did not have all characteristics of the summertime jet over the Great Plains. Also, the jet maximum varied with latitude because of the Coriolis parameter. On the other hand, observations showed that this variation is more applicable for wintertime jets. This study also investigated a soil-moisture factor on jet development and confirmed the results of the previous study.

Zhong et al. (1996) used the Regional Atmospheric Modeling System (RAMS, Pielke et al. 1992) and data from the NOAA wind profiler demonstration network to investigate the physical mechanisms responsible for the initiation, evolution, maintenance and decay of the LLJ.

The model results agreed fairly well with the observation of the LLJ. They showed that the frictional decoupling and inertial turning by the Coriolis force is more important for the formation of the LLJ than variation in horizontal pressure gradient. Increasing of the Coriolis parameter with latitude enhances the LLJ. They also ran a simulation with different soil moisture values and determined that soil moisture has an effect on the amplitude of the oscillation (drier soil, bigger amplitudes), but not a big influence on the phase.

The rapid growth of wind energy industry brought a renewed interest in LLJ phenomenon because high low-level wind speeds associated with LLJs are important for wind energy production and, at the same time, the presence of LLJs can significantly modify the vertical wind shear and nighttime turbulence in the vicinity of the wind turbine hub height and have detrimental effects on rotors. Thus, accurate predicting of LLJ is important for wind energy industry. The WRF model has been used for wind energy industries for local wind predictions and Storm et al (2009) evaluated the WRF model's ability to predict LLJs and their characteristics. The study concluded that the WRF model has the capability to capture some of the essential characteristics of the observed LLJ events, but also has the tendencies to overestimate LLJ heights and to underestimate LLJ wind speeds.

CHAPTER III

Objectives of the Current Study

As presented above, there have been numerous studies, both observational and numerical, on the LLJs characteristics and the mechanisms responsible for their formation and over the world. Southerly LLJs over the Great Plains of the United States are the most studied of all. Some of those studies are based on observations (Pitchford and London 1962; Frisch et al. 1992) while others are based on model outputs (McCorcle 1988; Fast et al. 1990; Zhong et al 1996). Almost all these studies have discussed different physical mechanisms that cause the occurrence of the SLLJ, but until only recently a few studies have examined the NLLJ (Whiteman et al. 1997; Walters et al. 2008). These studies brought new information about NLLJ climatology, but none of them examined physical mechanisms related to the NLLJ occurrence and development. These studies all concluded that future studies needs to take closer look into the northerly LLJ phenomena.

In the present study, two NLLJ episodes developed under different synoptic conditions were simulated using the Weather Research and Forecast (WRF) model (Skamarock et al. 2008). The objectives of the study are:

- 1) To assess the skill of the WRF model for simulating NLLJs and provide guideline on optimal model setting
- 2) To depict the detailed spatial and temporal characteristics of the NLLJ
- To better understand the large-scale environments and their interactions with regional and local forcing for the formation of NLLJ

CHAPTER IV

Data and Methodology

Case Selection

In this study, we first used twice daily rawinsonde data to diagnose the presence of the northerly low-level jet at the station. Following Walters (2001), we define a NLLJ as the following: a wind speed maximum of at least 8 ms⁻¹ between the surface and 700 hPa, a minimum decrease in wind speed of 4 ms⁻¹ below the jet maximum, and above the level of maximum wind speed to the next minimum or 550 hPa (whichever was located lower in the atmosphere), and a wind direction between 293-67° at the level of the maximum wind speed.

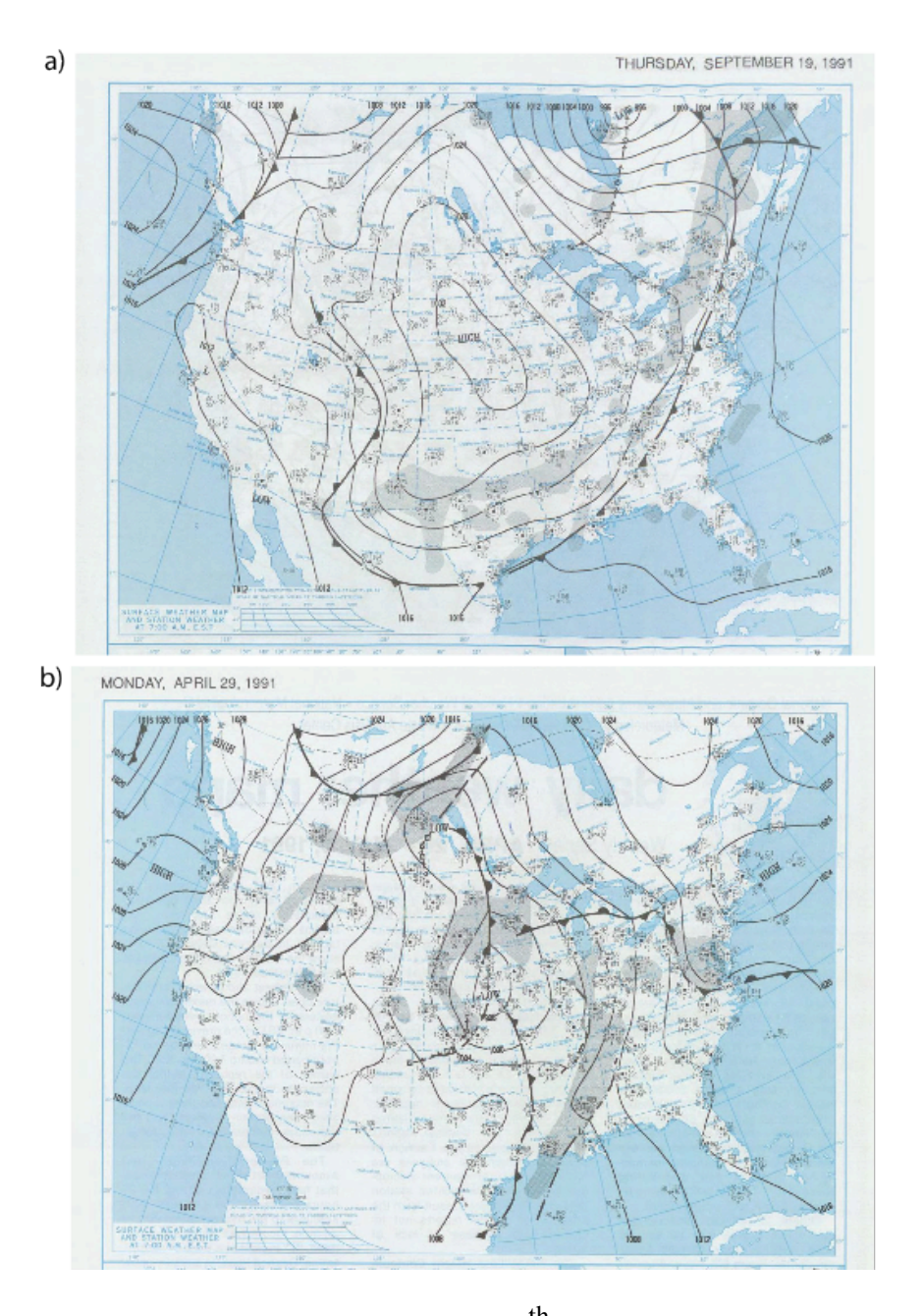


Figure 1. Surface weather charts for a) September 19th, 1991 at 7 a.m. local time, and b) April 29th, 1991 at 7 a.m. local time. "For interpretation of the references to color in this and all other figures, the reader is referred to the electronic version of this thesis (or dissertation)."

Based on the analyses of the rawinsonde soundings from the south-central Great Plains, two NLLJ cases with very different synoptic environments were selected for this study. The first NLLJ case, which occurred on 19-20 September 1991, was associated with a large high-pressure system centered over central US (Fig. 1a). The broad anticyclone covered nearly the entire US, with cold front on its periphery, heading southward towards the Gulf of Mexico and eastward towards the Atlantic Ocean. At 00 UTC September 19, six rawinsonde stations reported a NLLJ, with maximum wind speed of 17 ms⁻¹. With the strengthening of the surface anticyclone at 12 UTC, two more stations also reported NLLJ and maximum jet speed of approximately 20 ms⁻¹ of this event was reported at Norman Westheimer, Oklahoma (OUN; 35.23 °N, 97.47 °W) at the elevation of 888 hPa (Fig. 2a). At OUN, the wind rotated from the surface to higher elevations in a counterclockwise direction, with north-northeasterly winds below 800 hPa, shifting to northwesterly up to 650 hPa, and to westerly above that. On the following day (September 20), NLLJ profiles were observed at five stations at 00 UTC, and at ten stations at 12 UTC with measured maximum wind speed of approximately 15 ms⁻¹.

The second NLLJ case occurred on April 29, 1991. In contrast to the first case, the synoptic environment for this case was characterized by a mid-latitude cyclone that was centered on the four-state (Kansas, Nebraska, Iowa and Missouri) corner, with a surface pressure of 996 hPa (Fig. 1b). The cyclone was at mature stage with a well-defined cold front extending from the center southward to the Gulf of Mexico, a stationary front extending eastward across the Great Lakes states, and an occluded front extending northward to another low over Canada.

Sounding stations on the western and southwestern side of the cyclone reported NLLJ with peak wind speed generally occurring near 800 hPa level. The strongest low-level maximum of 28 ms⁻¹ at 801 hPa was reported at 12 UTC April 29 at North Platte (LBF) of Nebraska (Fig. 2b) just next to the cyclone center. In the next 6 hours, the jet is displaced away from the center to the periphery, with maximum wind speed decreasing to 24 ms⁻¹. Compare to the September case described above, the maximum wind speed is stronger and occurred at higher level, and the minimum wind speed above the jet nose appeared around 550 hPa which was also significantly higher than 780 hPa where the wind speed minimum was found in the September case. Another noticeable difference between the two cases lies in how the wind direction shifted with height. In the previous case, the wind rotated counterclockwise from surface to higher levels, but in this case, the wind rotated clockwise with height, with north-northwesterly wind below 650 hPa, turning to northwesterly until 300 hPa, and to southerly above that.

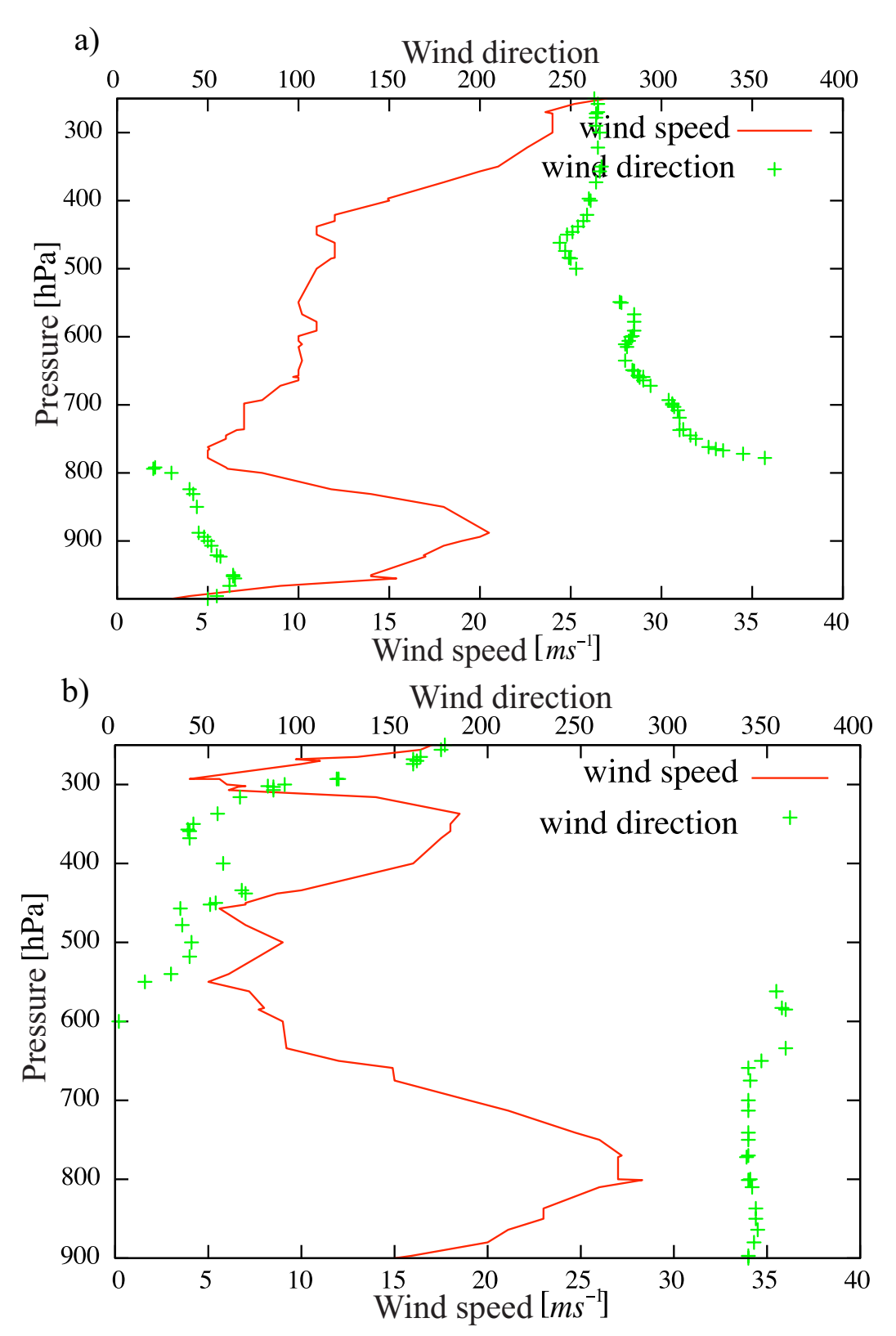


Figure 2. Rawinsonde observations of wind speed and direction taken at a) 12 UTC, 19 September, 1991 from the OUN station, and b) at 12 UTC, 29 April, 1991 from the LBF station.

Model and setup

Although the rawinsonde observations can reveal the vertical structure of NLLJs, the sounding sites are separated by an average distance of 350 to 450 kilometers and at each site soundings are launched only twice daily. Such coarse spatial- and temporal-resolution observations make it difficult to examine the spatial variation and the time evolution of the NLLJs. The limited observations also make it hard to fully understand the physical processes involved in the development of these NLLJs. A mesoscale numerical model is, thus, used here to describe the NLLJ structure at finer spatial and temporal resolution and provide insight into physical and dynamical processes responsible for the formation and evolution of the jet.

In the current study, the Weather Research and Forecasting (WRF) Model (v3.2.1) Advance Research WRF core (ARW) is used to simulate the two NLLJ cases described above. The WRF ARW model is a mesoscale, nonhydrostatic model, with a terrain-following pressure coordinate and an Arakawa C-grid. The model can be run in both idealized and real case modes and for real case the model can be driven by several large-scale analyses fields. The model supports several nested options including one-way, two-way and moving nest grids. In the current study, three nested grids are used. The outermost grid has a horizontal grid spacing of 36 km and 100 by 100 grid points encompassing the entire contiguous United States (22-54 °N and 126-72 °W). The middle grid has a grid resolution of 12 km, and a domain size of 1812 km x 1812 km (151 X 151 grid points) covering central US. Finally the innermost grid was placed over the south-central Great Plains with a horizontal grid spacing of 4 km and a domain size of 844 km by 844 km (211 x 211 grid points). All three grids have the same vertical configuration with 60 vertical levels stretched from the surface to 100 hPa.

For this study, the initial and boundary conditions are provided by the North American Regional Reanalysis or NARR (Mesinger et al. 2006). NARR is a long-term, dynamically consistent, high-resolution atmospheric and land surface hydrology data set for the North American domain. The horizontal resolution of NARR is 32 km, which is comparable to the resolution of the outermost model grid, and the temporal resolution is 3 hourly.

To determine if the WRF model can be used as an appropriate tool for simulating the NLLJ episode, we compare the model results with the observations and the reanalysis data.

As a community model for both weather research and forecasting communities, the WRF model contains various user-specified options for physical parameterizations. One purpose of the study is to determine what combination of physical parameterizations gives the best performance of WRF for simulating NLLJ events. A series of simulations are, thus, performed with various combinations of parameterization schemes for cloud microphysics, cumulus convection, boundary-layer turbulence, and land surfaces. Table 1 lists the parameterization schemes used for nine simulations. The same radiation scheme (CAM, Collins et al., 2004) was used for both shortwave and longwave radiation calculations for all simulations.

Table 1. List of physical parameterization schemes used by each model run

Runs	Cloud microphysics scheme	Land surface model	Boundary layer turbulence scheme	Cumulus scheme
WSM5- Noah-MYJ	WRF Single- Moment (WSM) 5- class scheme	Noah	Mellor-Yamada- Janjic TKE	no
WSM6- Noah-MYJ	WSM 6-class graupel scheme (scheme with ice, snow and graupel processes)	Noah	Mellor-Yamada- Janjic TKE	no

Table 1 (cont'd)

WSM5- Noah-MYJ- KF	WRF Single- Moment (WSM) 5- class scheme	Noah	Mellor-Yamada- Janjic TKE	Kain- Fritsch
WSM5- Noah-MYJ- BMJ	WRF Single- Moment (WSM) 5- class scheme	Noah	Mellor-Yamada- Janjic TKE	Betts- Miller- Janjic
WSM5- Noah- MYNN-KF	WRF Single- Moment (WSM) 5- class scheme	Noah	MYNN 2.5 level TKE	Kain- Fritsch
WSM5- Noah- BouLac-KF	WRF Single- Moment (WSM) 5- class scheme	Noah	Bougeault and Lacarrere (BouLac) PBL	Kain- Fritsch
WSM5-TD- MJY-KF	WRF Single- Moment (WSM) 5- class scheme		Mellor-Yamada- Janjic TKE	Kain- Fritsch
WSM5- RUC-MYJ- KF	WRF Single- Moment (WSM) 5- class scheme	RUC	Mellor-Yamada- Janjic TKE scheme	Kain- Fritsch
WSM5-PX- ACM2-KF	WRF Single- Moment (WSM) 5- class scheme		ACM2 (Pleim) scheme	Kain- Fritsch

Details on the physical parameterizations listed in the table above are given in the Appendix A.

CHAPTER V

Results

The results of the WRF simulations are discussed here and the discussions are organized by case. Each case will begin with synoptic analyses, followed by model results.

April case

Synoptic Analysis

The April episode was marked by a cyclone that was centered over north-central Great Plains. As shown in Figure 3, at 00 UTC on April 29, 1991, 12h hours before the jet is observed at LBF station, air above the southern Plains is generally warm and moist, coming for the south, but in the next 12 hours it is replaced with cold and dry air coming from the northwest, creating strong temperature gradient over the region. The surface Low over the southern Great Plains deepens on its transition from southwest to northeast cross the central US. Over the 24-hour period, the center pressure drops from 1004 hPa to 996 hPa. Cold air from west makes its transition toward east at the back side of the surface Low.

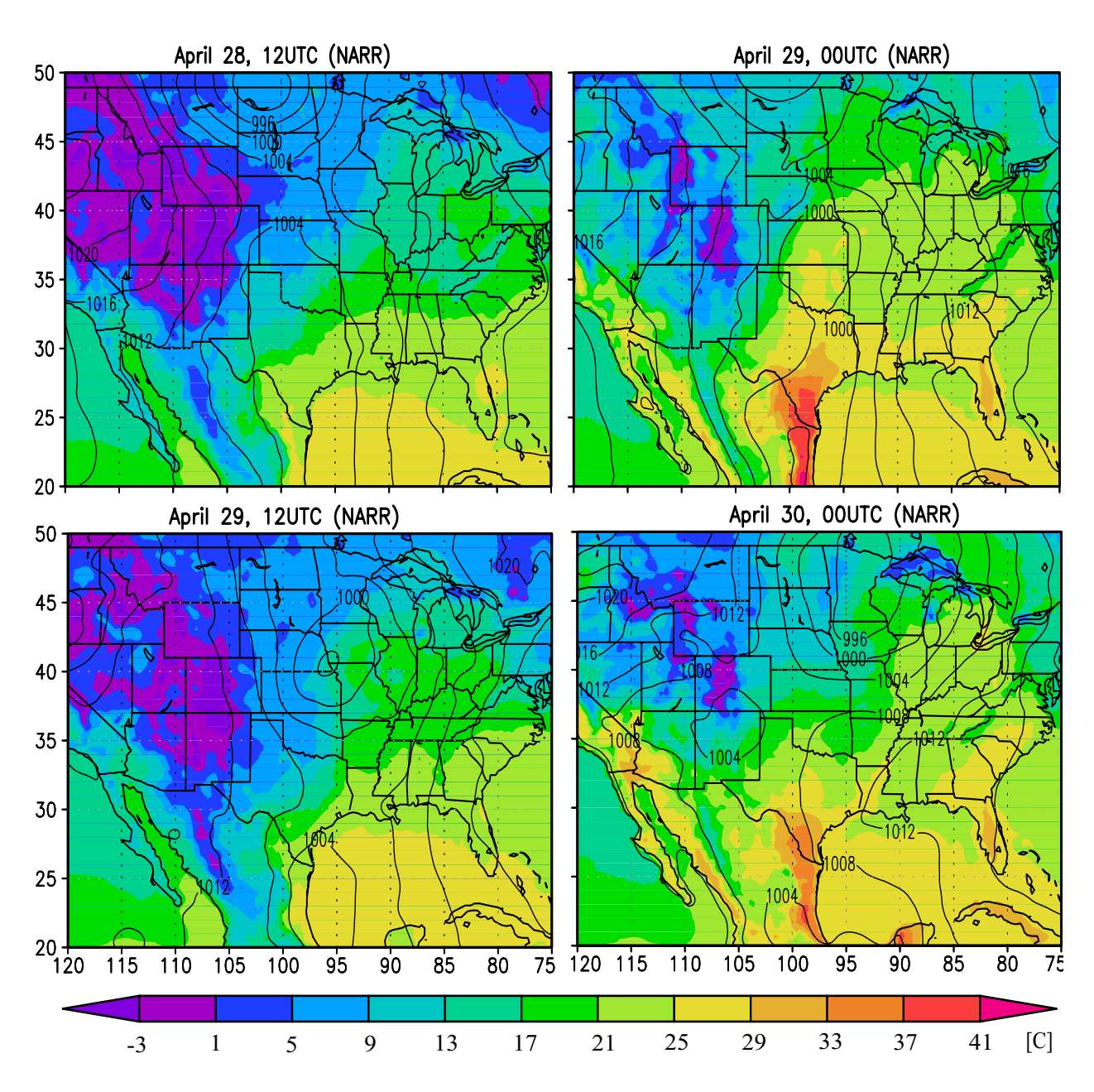


Figure 3. Distributions of the NARR-derived mean sea-level pressure and temperature (top panel), 800 hPa geopotential height, temperature and wind speed (middle panel), and 250 hPa geopotential height and winds (bottom panel) for April 28-30, 1991.

Figure 3 (cont'd)

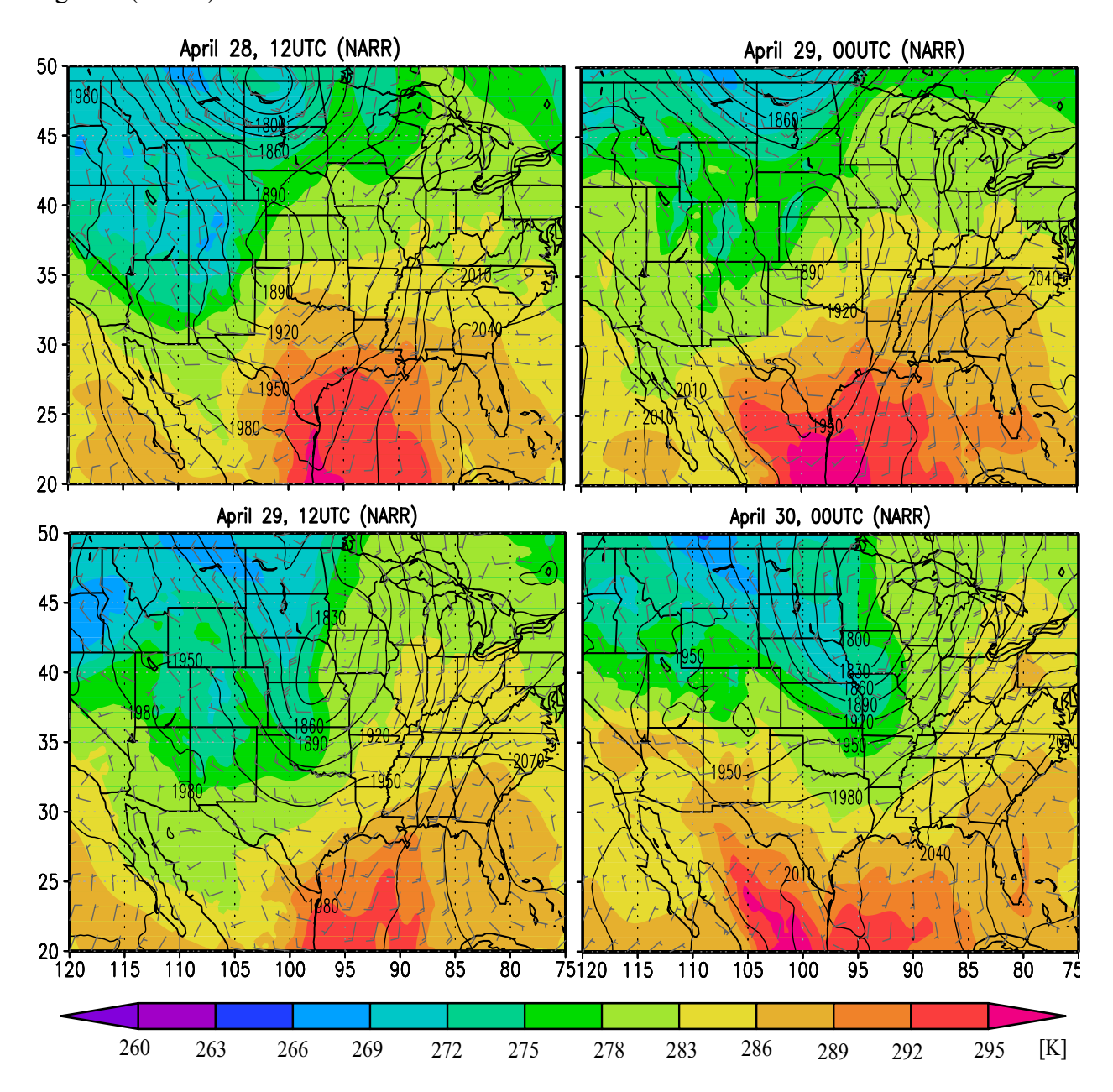
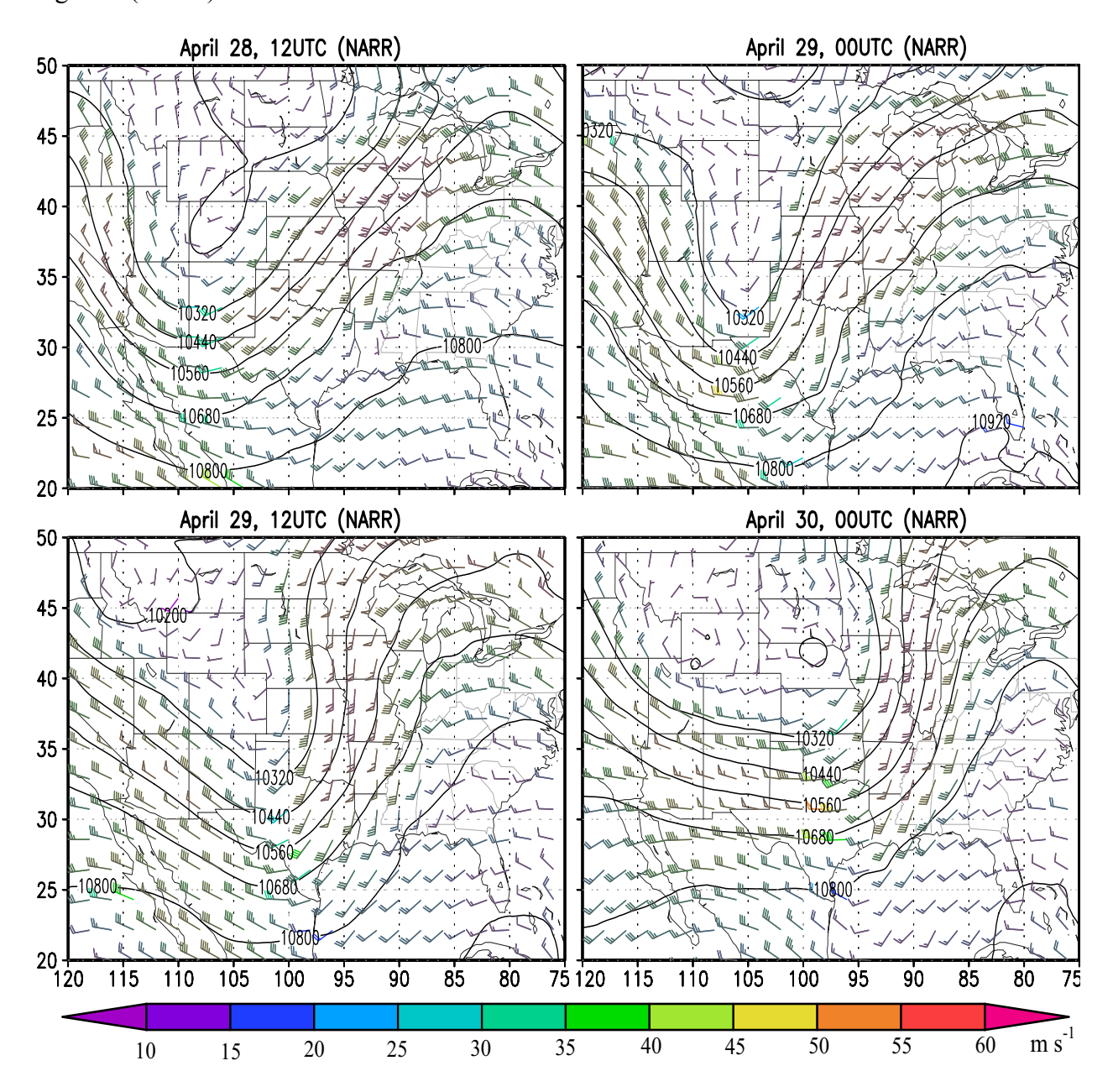


Figure 3 (cont'd)



During the same period, an elevated Low centered over Kansas-Oklahoma border deepens and moves northeastward (Figure 3, middle panel). Cold air from northwest is sucked in by a clockwise rotation, transporting cold air southward up to northern Oklahoma and Arkansas.

Further up at 250 hPa upper-level trough exists and the axis of trough changes from negative (tilted toward east) at the beginning of the period at 12 UTC on April 28, to positive

(tilted toward west) later at 12 UTC on April 29. This change tightens the geopotential height lines and the stronger gradient leads to an acceleration of winds.

WRF simulation

As described early in model setup in Chapter IV, nine WRF simulations were performed with different combinations of physical parameterizations. To determine how sensitive that WRF simulations to the physical parameterizations, Figure 4 shows the simulated vertical profiles of wind speed taken from the grid point nearest to OUN at 12 UTC on September 19 and the simulated vertical profiles of wind speed taken from the grid point nearest to LBF at 12 UTC on April 29 from all nine simulations. Despite the different combinations of the physical parameterization schemes used for the runs, the simulated jet profiles show only small differences among the runs and the differences are mostly in upper levels. This result suggests that the NLLJ simulations do not heavily depend on the specific parameterizations chosen.

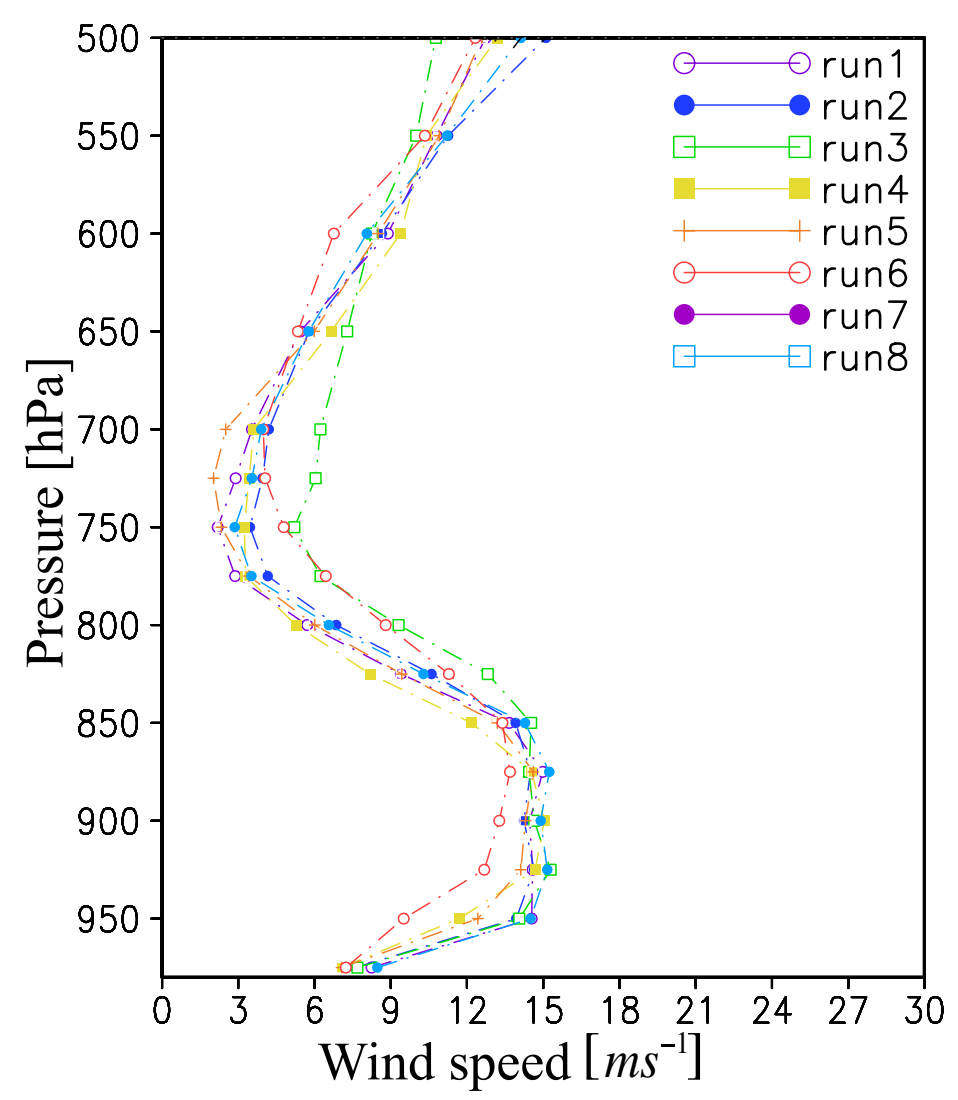
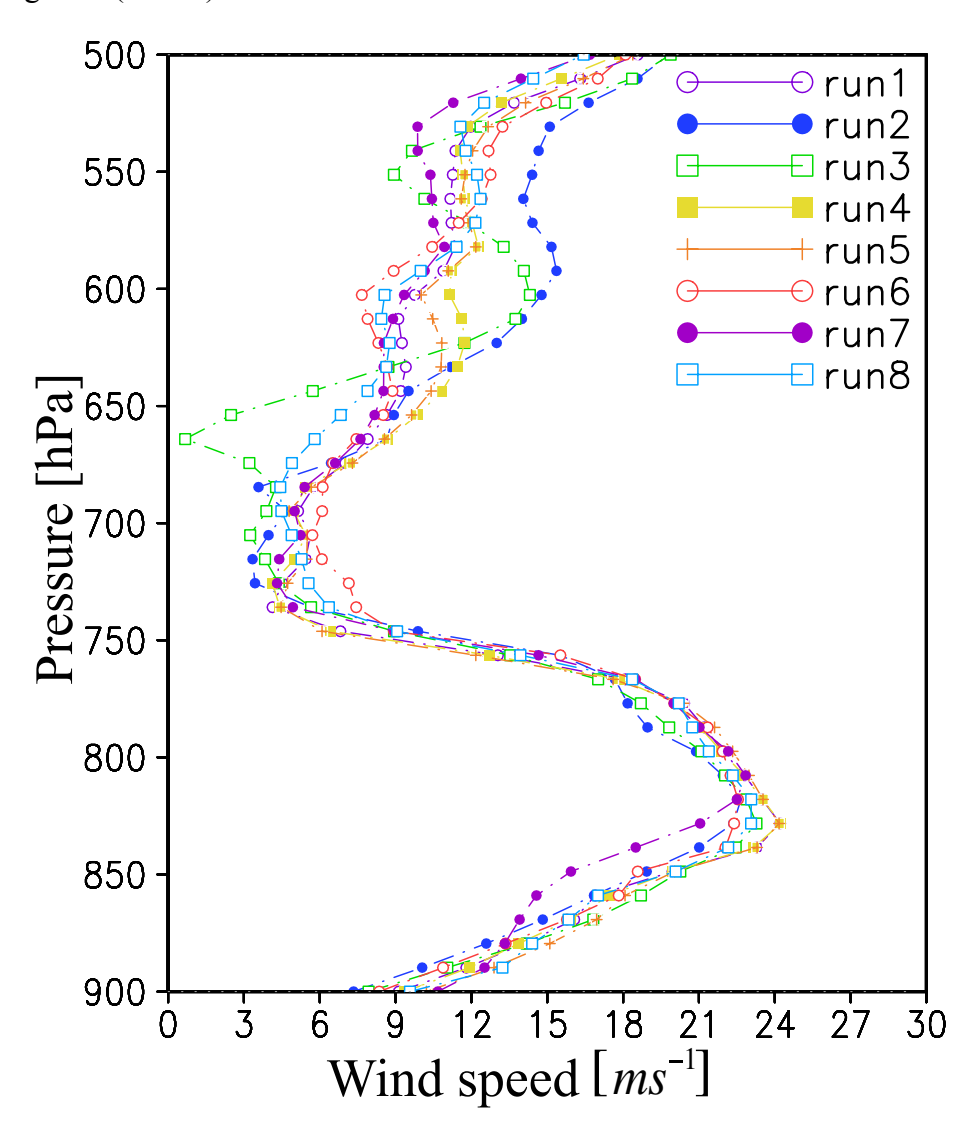


Figure 4. Vertical profiles of wind speed simulated by WRF using different physical parameterizations taken from the innermost grid from the model grid point closest to the OUN station at 12 UTC, September 19, 1991 (up), and from the model grid point closest to the LBF station at 12 UTC, April 29, 1991 (bottom).

Figure 4 (cont'd)



Therefore, for the further analysis, we choose the results from the simulation 4 that used WSM 5 mircophsyics scheme, Betts-Miller-Janijic convective scheme, MYJ PBL scheme and Noah land surface model.

First, we compare the model simulated large-scale environments (Figure 5) with the NARR derived fields (Figure 3).

For the April case, the simulated pressure patterns (Figure 5) are in good agreement with pressure pattern plotted from the NARR (Figure 3). The simulation placed the low pressure center slightly south of the observed positions, but the center pressure value is simulated well. The model also appears to capture the upper-level features quite well. At 800 hPa, the center of the elevated low is located over northern parts of Kansas and eastern part of Nebraska. At the same time, temperature changes from 266 K in the northwestern part of the domain, to 290 K in the southeastern part. At the 250 hPa, low wind speeds are located over Wyoming and Colorado, while highest wind speeds are located on the east side of the trough over Missouri and Iowa.

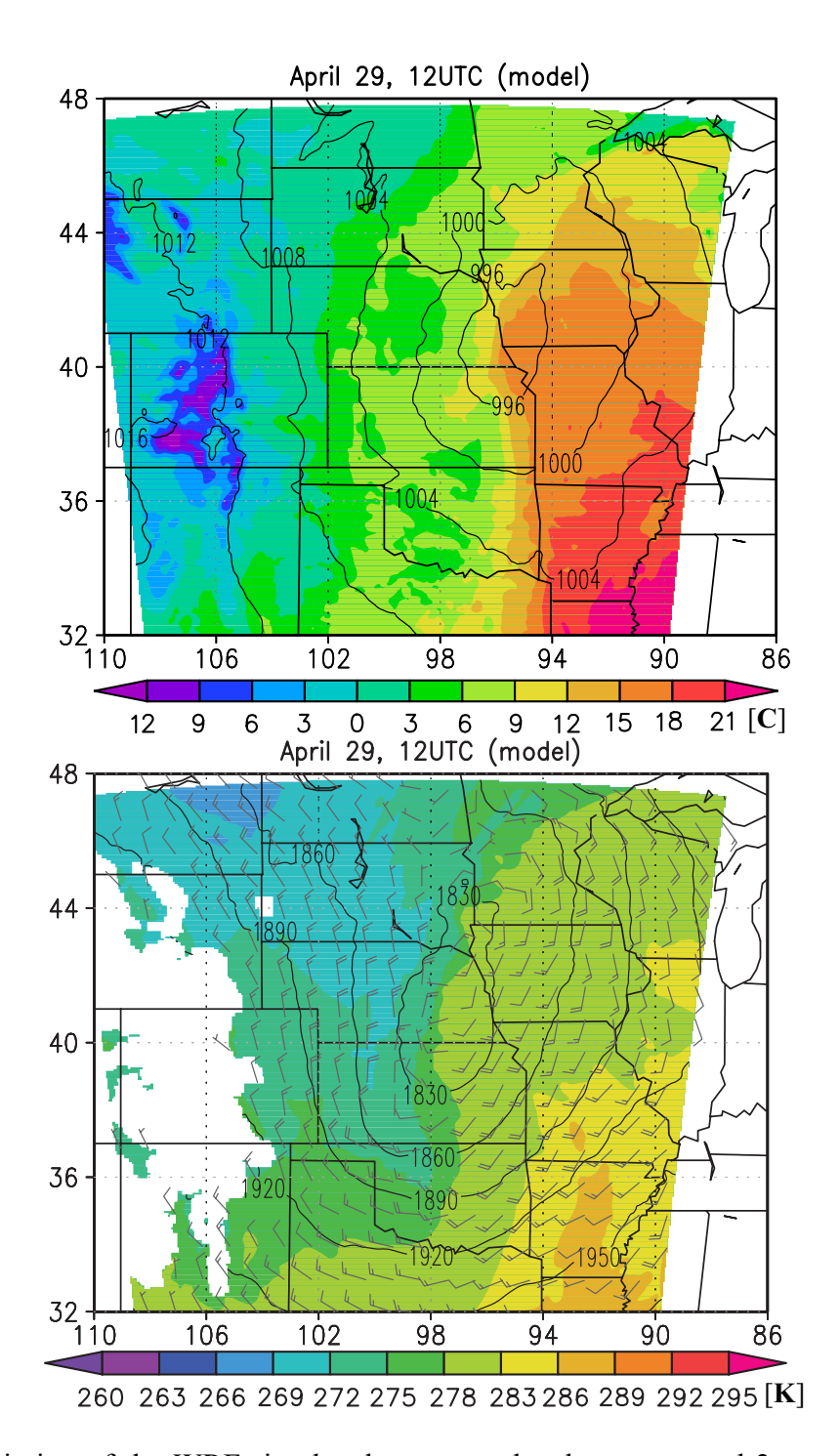


Figure 5. Distriution of the WRF-simulated mean sea-level pressure and 2 m temperature, 800 hPa geopotential height and temperature, 250 hPa geopotential height and wind speed for 12 UTC, April 29, 1991.

Figure 5 (cont'd)

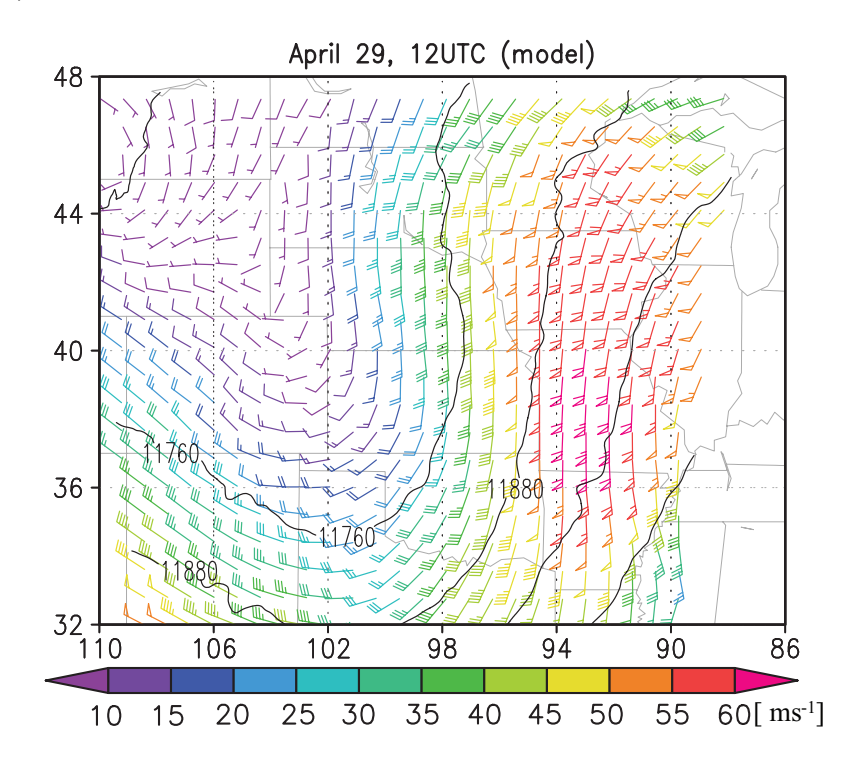


Figure 6 shows the simulated, rawinsonde and NARR-derived wind profiles at the North Platte station, at 12 UTC on April 29, 1991. Both WRF and NARR profiles capture the vertical structure of the rawinsonde profile. The maximum rawinsonde observed jet speed is 27 ms⁻¹, compared to 22 ms⁻¹ in the WRF simulation, an underestimation of 18%. Similar underestimations of 10-30% in the simulated maximum jet speed are also found at several other rawinsonde station locations. The vertical wind shear below and above the jet nose is also underestimated by the model. But WRF has successfully simulated the minimum wind speed above the jet nose and the secondary wind maximum aloft at around 350 hPa. WRF simulated wind direction is also in very good agreement with the observed. NARR has also underestimated the maximum jet speed, although its value (23 ms⁻¹) is slightly higher than that of WRF

simulation. At the higher levels, however, NARR is not capable of simulating the observed minimum wind speed and it also fails to capture the wind speed maximum at 350 hPa.

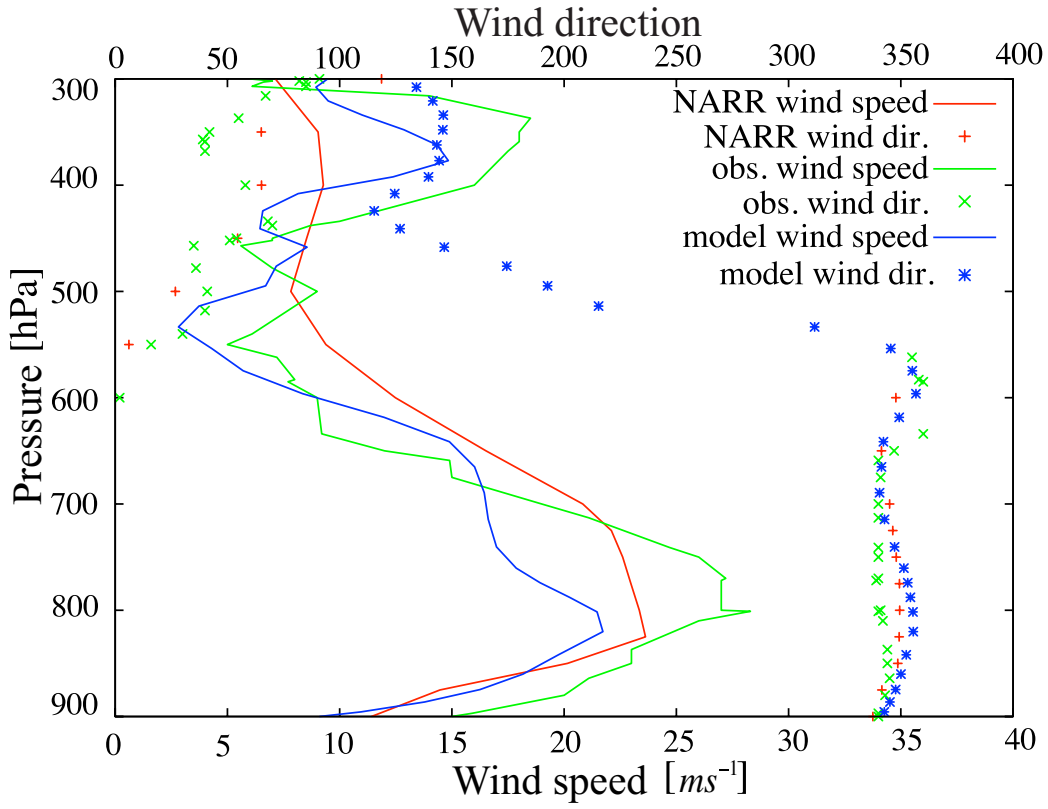


Figure 6. Modeled, observed and NARR vertical wind speed profiles at 12 UTC, April 29, 1991 at the LBF station.

With a horizontal resolution of 12 km, the simulation is able to depict in more detail the spatial distribution of the jet structure during a NLLJ episode than what rawinsonde observation network can provide. The vertical structure and the thermodynamic conditions of the atmosphere associated with the April NLLJ are examined using Figure 7. The mixing is strong as indicated by larger TKE values. The boundary-layer height grows from 200-300 m in early morning to 1500-3000 m around noon. The jet is located at the top of the mixed layer. At the west side of the surface Low, winds are predominantly from the north (blue shade), with a strong jet signature at 12 UTC, while at the east side of the surface Low winds are from the south (red shade). From

12 UTC to 18 UTC, temperature at the lowest levels where the surface Low is located changes from 291 K to 288 K, as the Low moves eastward and tilts more westward.

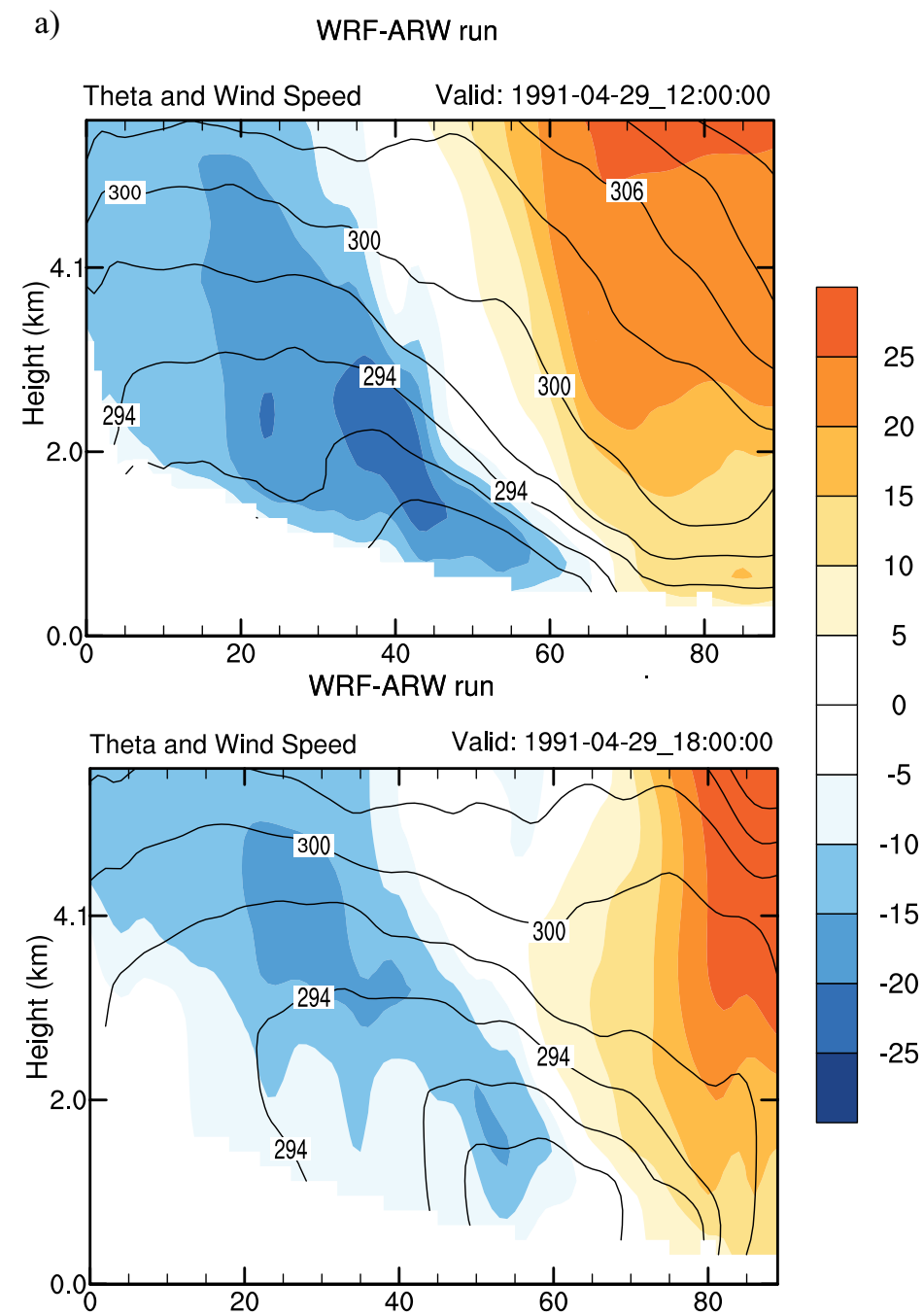


Figure 7. Cross sections of the simulated wind speed (shading) and contours of potential temperature (a) and turbulent kinetic energy (b) in the plane perpendicular to the jet core on at 12 and 18 UTC on September 19, 1991near the LBF station.

Figure 7 (cont'd)

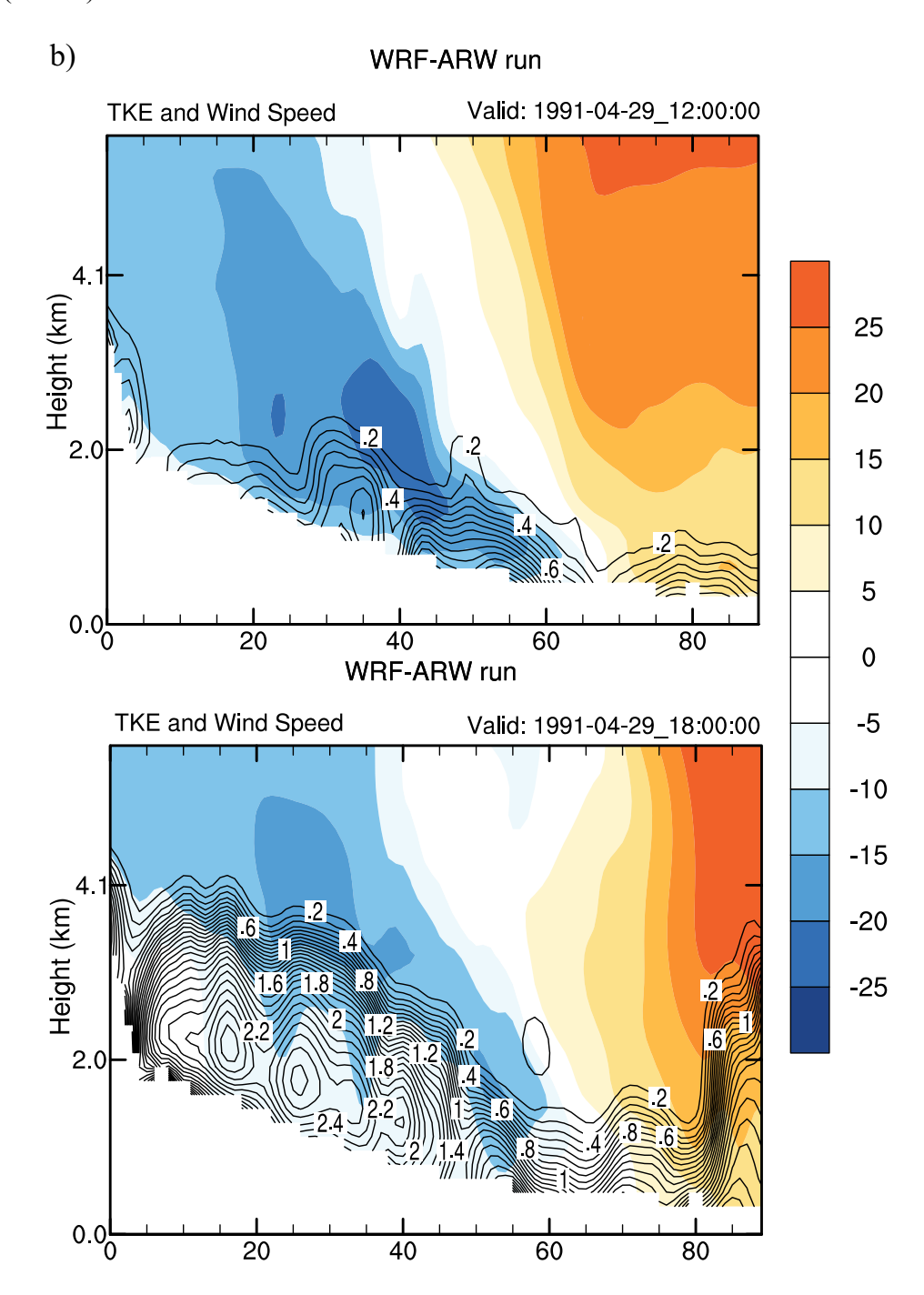


Figure 8 shows wind vector, potential temperature, and specific humidity at the maximum jet level in the case of the jet observed at 12 UTC on April 29. The temperature and moisture gradient in this case is oriented east-west with warm, moist air on the east side of the

cyclone where southerly flows prevailed, while dry, cool air to the west of the center of the cyclone where NLLJ occurred. As the NLLJ intensified rapidly between 06 and 12 UTC on April 29, the central part of the domain experienced rapid cooling and drying. As the cyclonic flow ramped around the cyclone, a zone of very dry air appeared on the southeast side of the domain. By the April 30, at 00 UTC, the whole domain is filled with a dry air, with specific humidity only 2-3 g kg⁻¹ in the southwest part of the region, and 4-5 g kg⁻¹ in the north-east part of the domain.

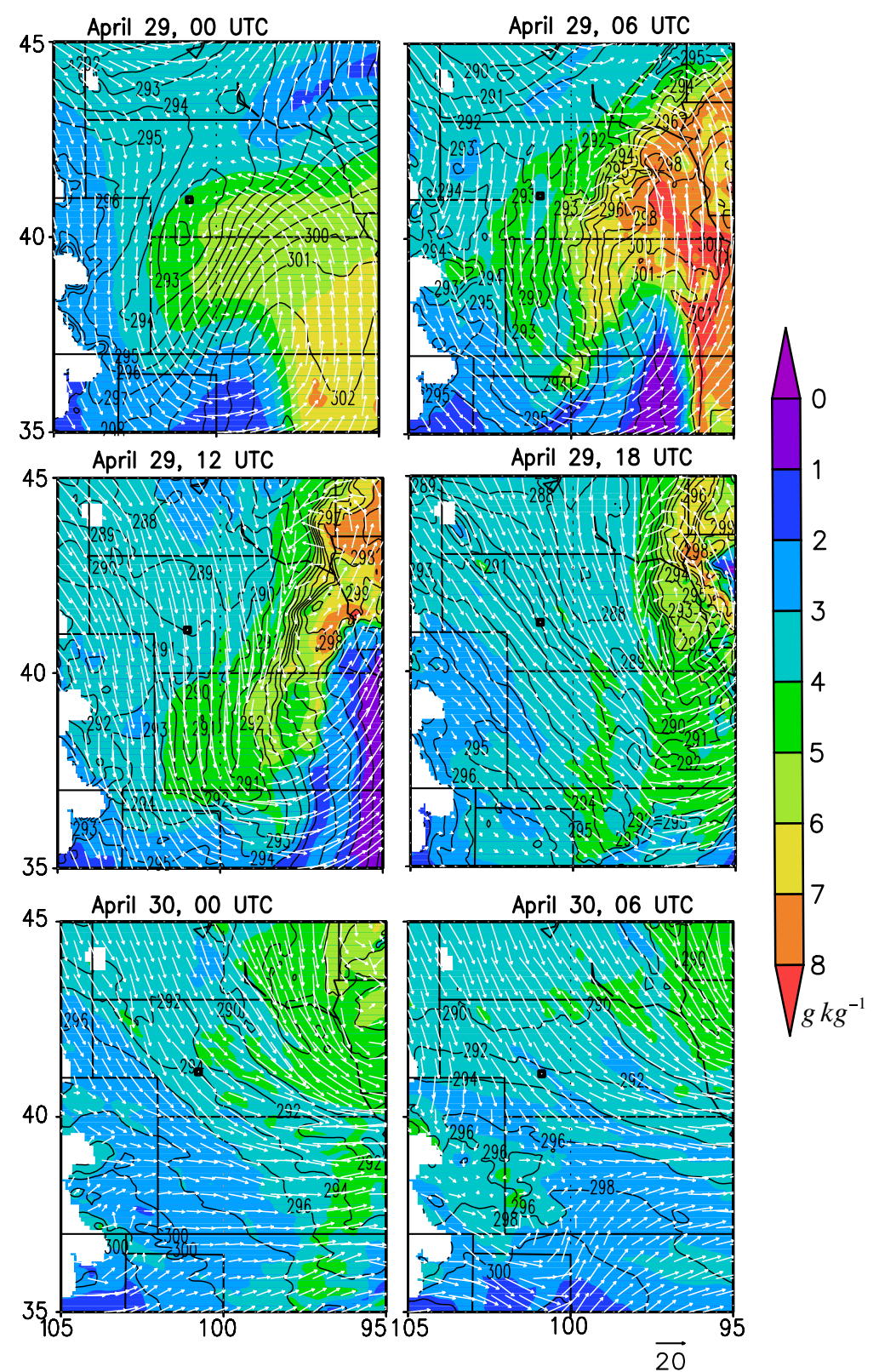


Figure 8. Distribution potential temperature (contours), specific humidity (shading) and wind vectors for 800 hPa pressure level between 00 UTC, April 29 and 00 UTC, April 30, 1991.

In the case of cyclonic flow (Figure 8), the temperature and moisture gradient was oriented east-west with warm, moist air on the east side of the cyclone where southerly flows prevailed, while dry, cool air to the west of the center of the cyclone where NLLJ occurred. As the NLLJ intensified rapidly between 06 and 12 UTC on April 29, the central part of the domain experienced rapid cooling and drying. As the cyclonic flow ramped around the cyclone, a zone of very dry air appeared on the southeast side of the domain. By the April 30, at 00 UTC, the whole domain is filled with a dry air, with specific humidity only 2-3 g kg⁻¹ in the southwest part of the region, and 4-5 g kg⁻¹ in the north-east part of the domain.

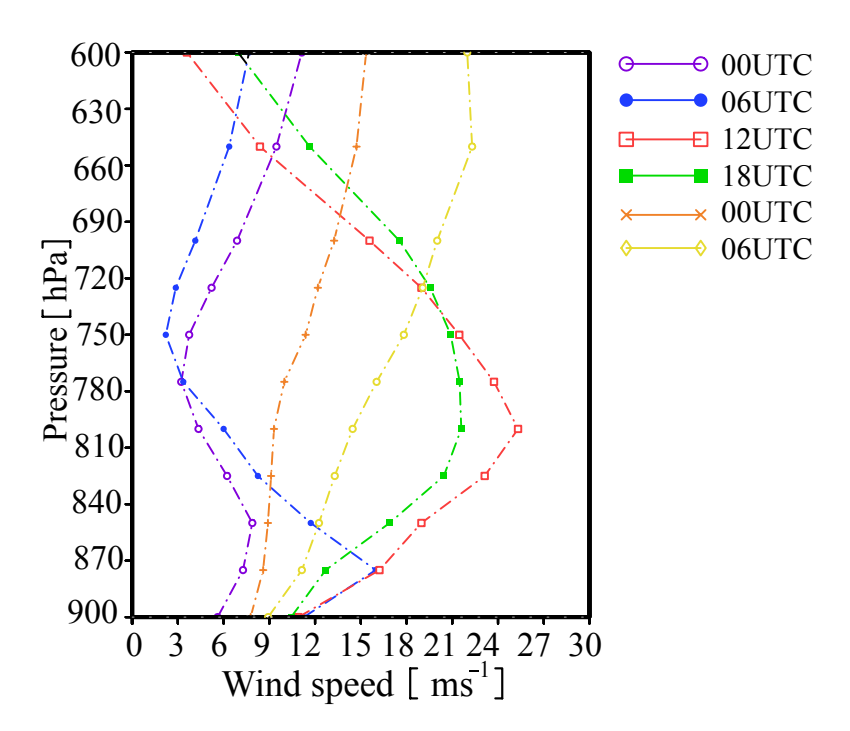
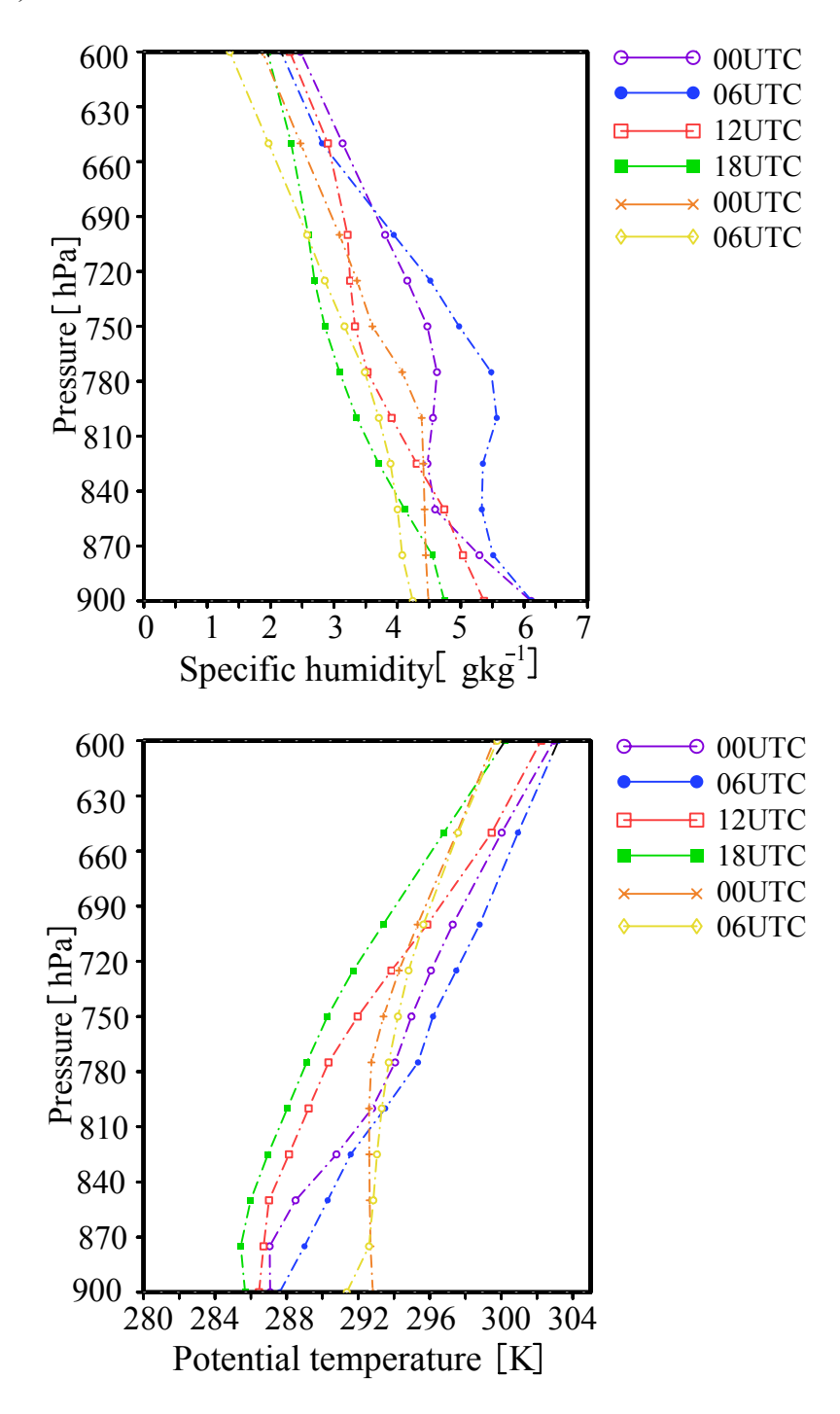


Figure 9. Vertical profiles of simulated wind speed, specific humidity and potential temperature at LBF station on 29 April, 1991.

Figure 9 (cont'd)



The time variation of vertical wind profiles, specific humidity and potential temperature are shown in Figure 9 from the model grid point nearest to LBF for the cyclone case. In the April

case, the jet began to form at 06 UTC on 29 April with a maximum wind speed of about 16 ms⁻¹ at 870 hPa. In the next 6 hours, the wind speed increased rapidly to a maximum of nearly 27 ms⁻¹ while the height of the wind maximum also raised up to about 800 hPa. The maximum speed dropped to 23 ms⁻¹ at 18 UTC with the broadening of the jet nose, and by 00 UTC 30 April, the profile completely lost the jet signature. The drying of the atmosphere was small, while there was a larger change in potential temperature with cooling between 0600 to 1800 UTC, followed by considerable warming afterwards.

September case

Synoptic Analyses

The synoptic conditions accompanying this case are quite different from that of the April case. The September episode is characterized by a large anticyclone that was centered over north-central Great Plains (Figure 10). On September 18, at 12 UTC, a surface Low was located north of the Great Lakes, while a High was located over Montana, Idaho and Wyoming. In the next 12-24 hours, the surface Low with center pressure of 1005 hPa, was moved toward northeast, while the High was moved farther to the east and south with itscenter pressure increasing from 1026 hPa to 1030 hPa. The east and southward movement of the High was accompanied by breakthrough of cold air from Canada to the central and southern Plains with the leading edge of the cold air reaching as far south as Kansas and Missouri.

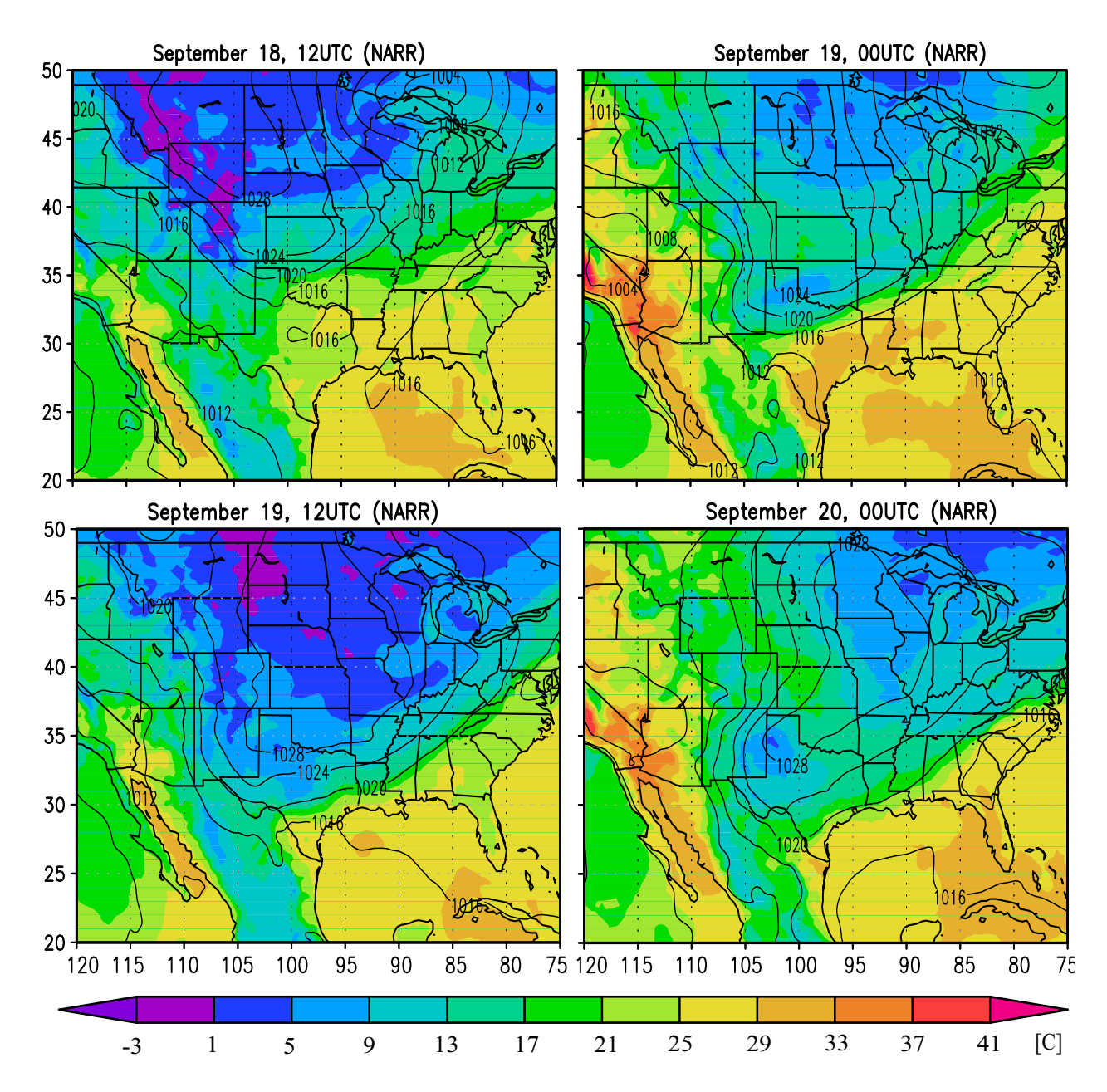


Figure 10.Distribution of the NARR-derived mean sea-level pressure and temperature (top panel), 900 hPa geopotential height, temperature and wind speed (middle panel), and 250 hPa geopotential height and wind speed (bottom panel) for September 19-20, 1991.

Figure 10 (cont'd)

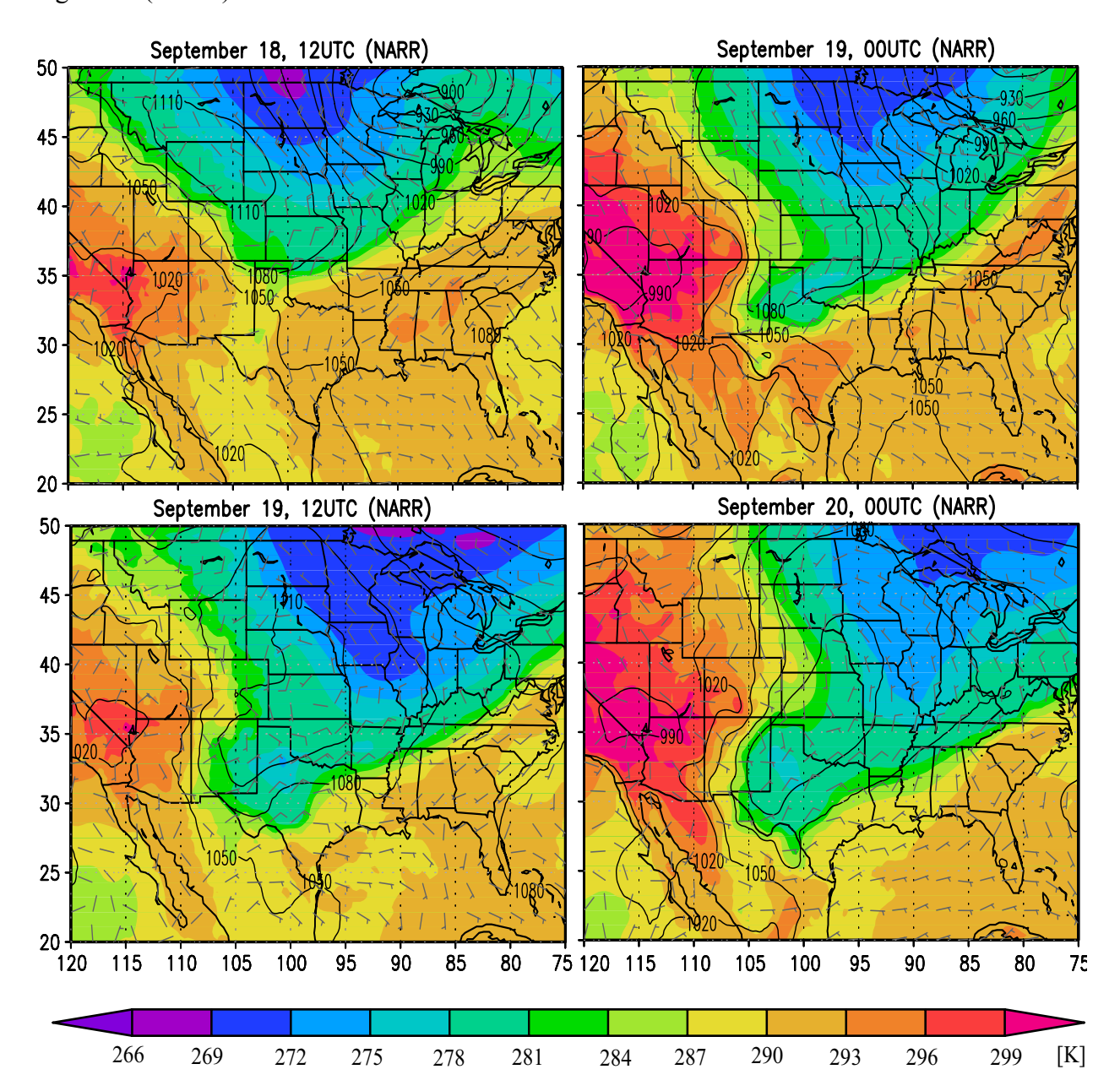
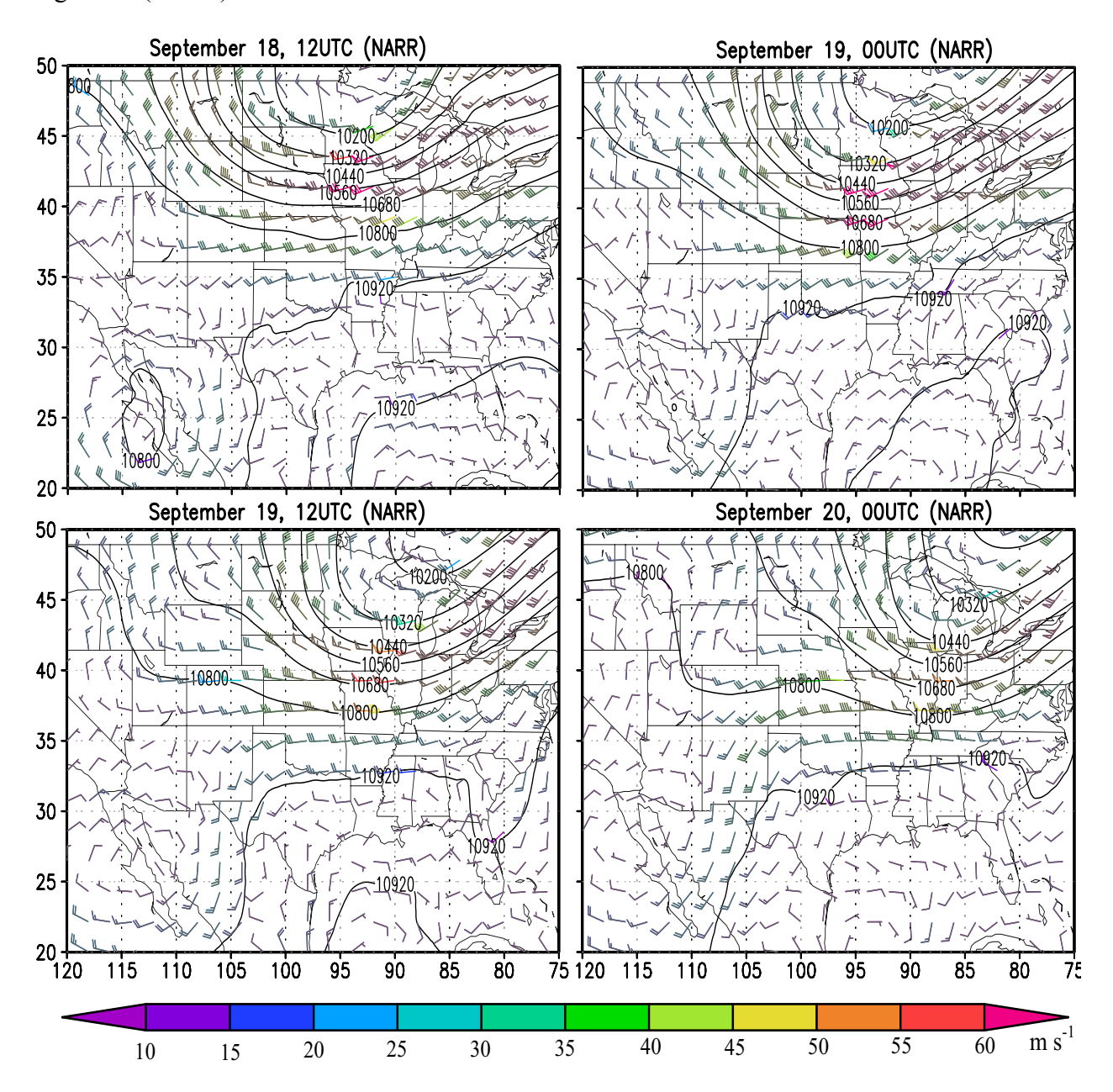


Figure 10 (cont'd)



The main feature on the 900 hPa charts is a developing upper-level Low located over the Great Lakes. Cold air from the north, with wind speeds of 40 ms⁻¹, wrapped around the Low, blowing parallel to isohypses. A pool of cold air was located next to the elevated Low, while warm air was present over the west coast, the southeast and the east coast of the United States.

Over the next 24 hours, the elevated Low progressed northeastward, and at the same time, the High deepened. By September 20th, warm air covered the entire western part of the domain, and the pool of cold air was situated over the Great Lakes.

The main feature of the 250 hPa map was an upper-level jet and upper-level through located over the northern states and southern Canada. The LLJ was located further south from the upper-level jet.

WRF Simulation

For the September case, a comparison of patterns in Figure 11 with those in Figure 10 revealed that the model simulated both the magnitude and the position of the anticyclone quite well. At 12 UTC on September 19, a surface High with center pressure of 1028 hPa is located over the southern Great Plains. The 2-m temperature over the same region is between 0 and 12 °C. At 900 hPa, the 1110 ghm isoline stretches from northern Texas and western Missouri further to the north, with temperature about 280 K. Temperature over the southern parts of Texas and over the Gulf of Mexico are between 290 and 295 K. The 250 hPa map exhibits an area of low wind speeds over the Gulf of Mexico and southern Texas, with wind speeds increasing northward and highest wind speeds locating over Illinois and Indiana.

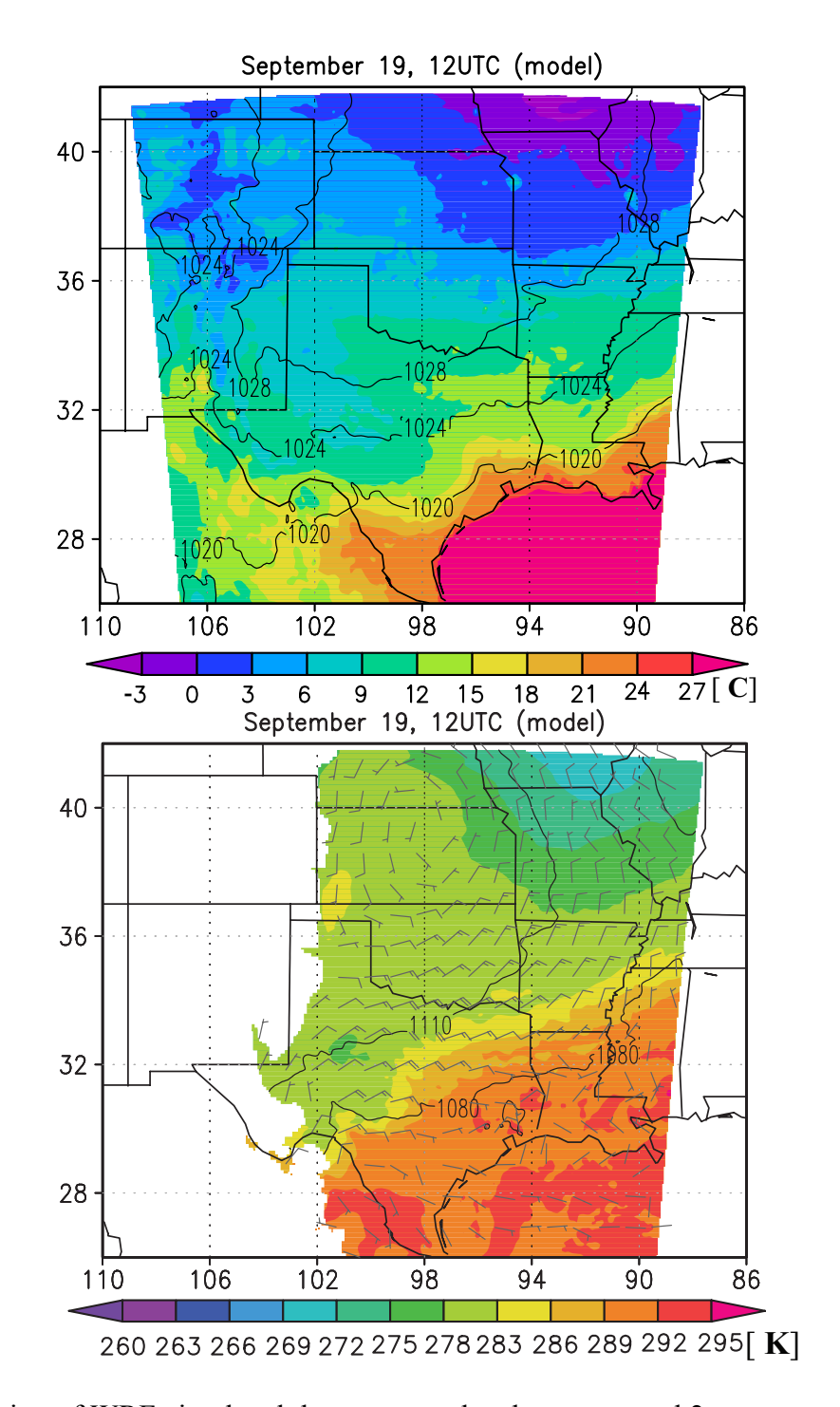
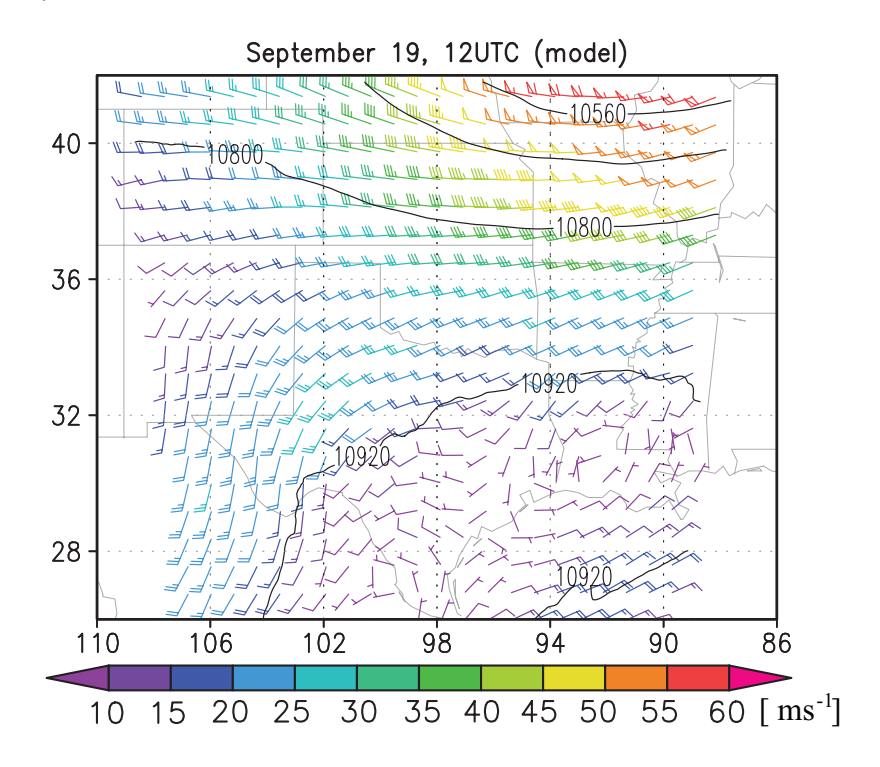


Figure 11. Distribution of WRF-simulated the mean sea-level pressure and 2 m temperature, 900 hPa geopotential height and temperature, 250 hPa geopotential height and wind speed for 12 UTC on September 19, 1991.

Figure 11 (cont'd)



To determine how well the model simulated LLJ, the simulated and observed wind profiles are compared at the rawinsonde location where the maximum jet wind speed was observed (Figure 12). The simulated profile is taken from the nearest grid point to the rawinsonde site (OUN). Both WRF and NARR capture quite well the vertical wind structure including the height where the maximum and minimum wind speed occur, but similar to the April case, the maximum wind speed at the nose of the jet is underestimated by both NARR and WRF and the jet nose is broader. The observed maximum wind speed is 20 ms⁻¹, compared to 14 ms⁻¹ of NARR and 17 ms⁻¹ of WRF. WRF did better than NARR possibly because of better resolution. The wind direction profiles from WRF and NARR are in excellent agreement with rawinsonde profile.

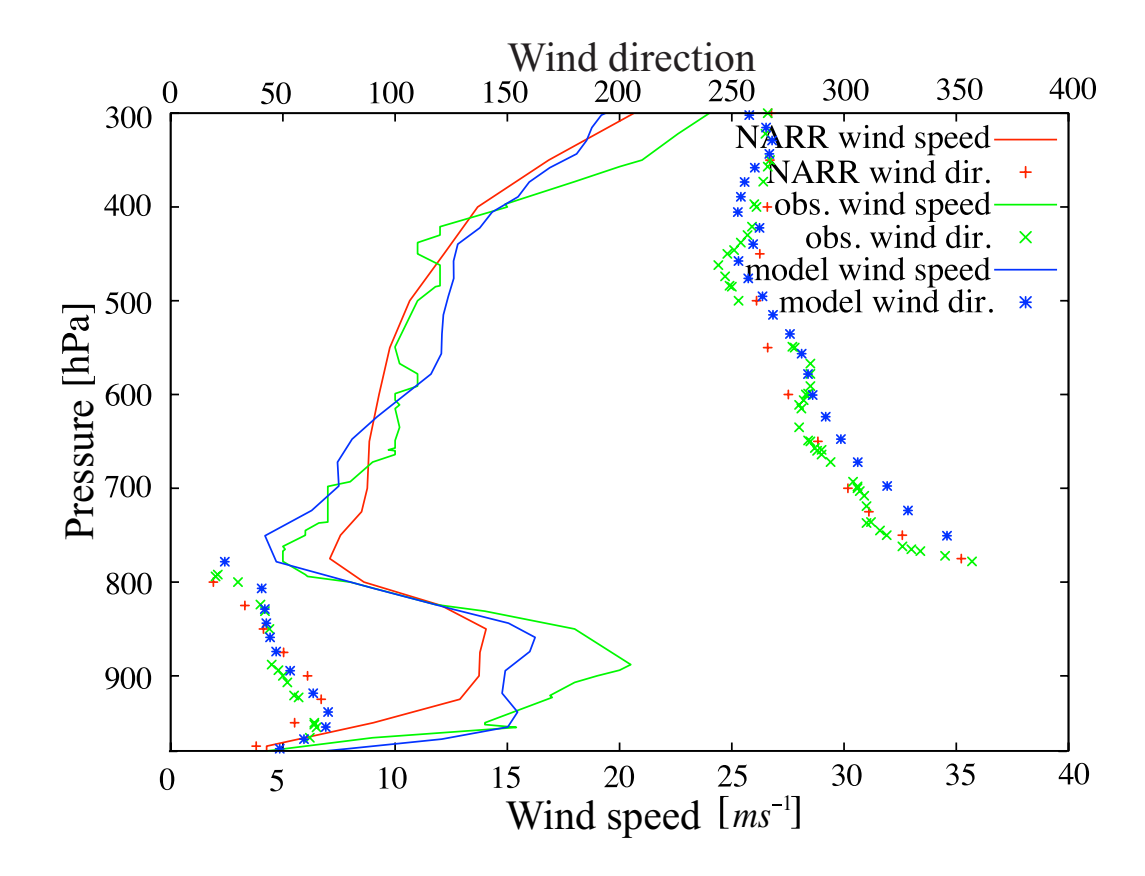


Figure 12. Modeled, observed and NARR vertical wind speed profiles at 12 UTC, 19 September 1991 at the OUN station.

The vertical NLLJ structure and the thermodynamic conditions of the atmosphere accompanying these NLLJs are examined using Figure 13 which shows the simulated wind speed, potential temperature, and turbulence kinetic energy (TKE) in the plane perpendicular to the jet core, with the center of cross sections through OUN.

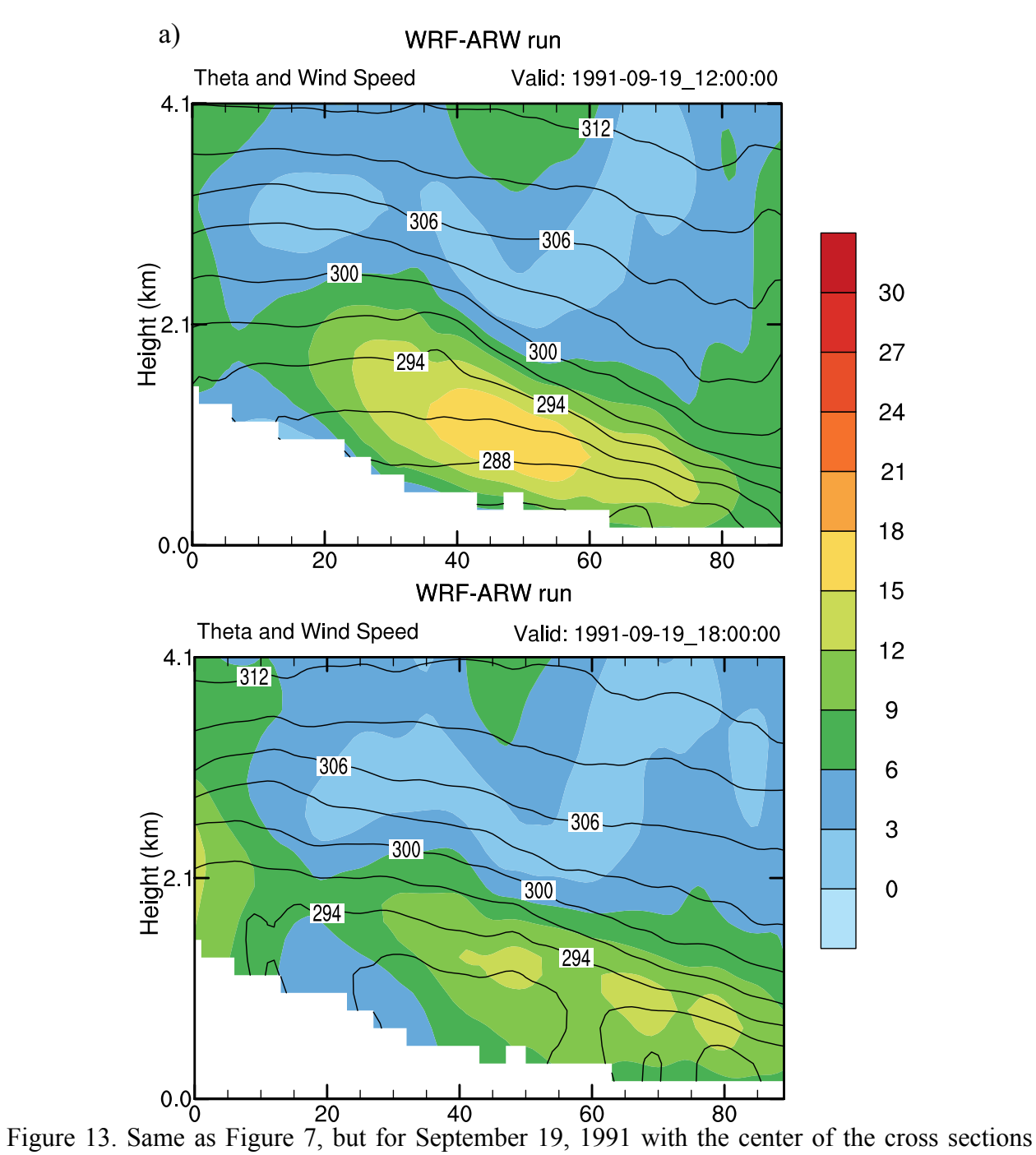
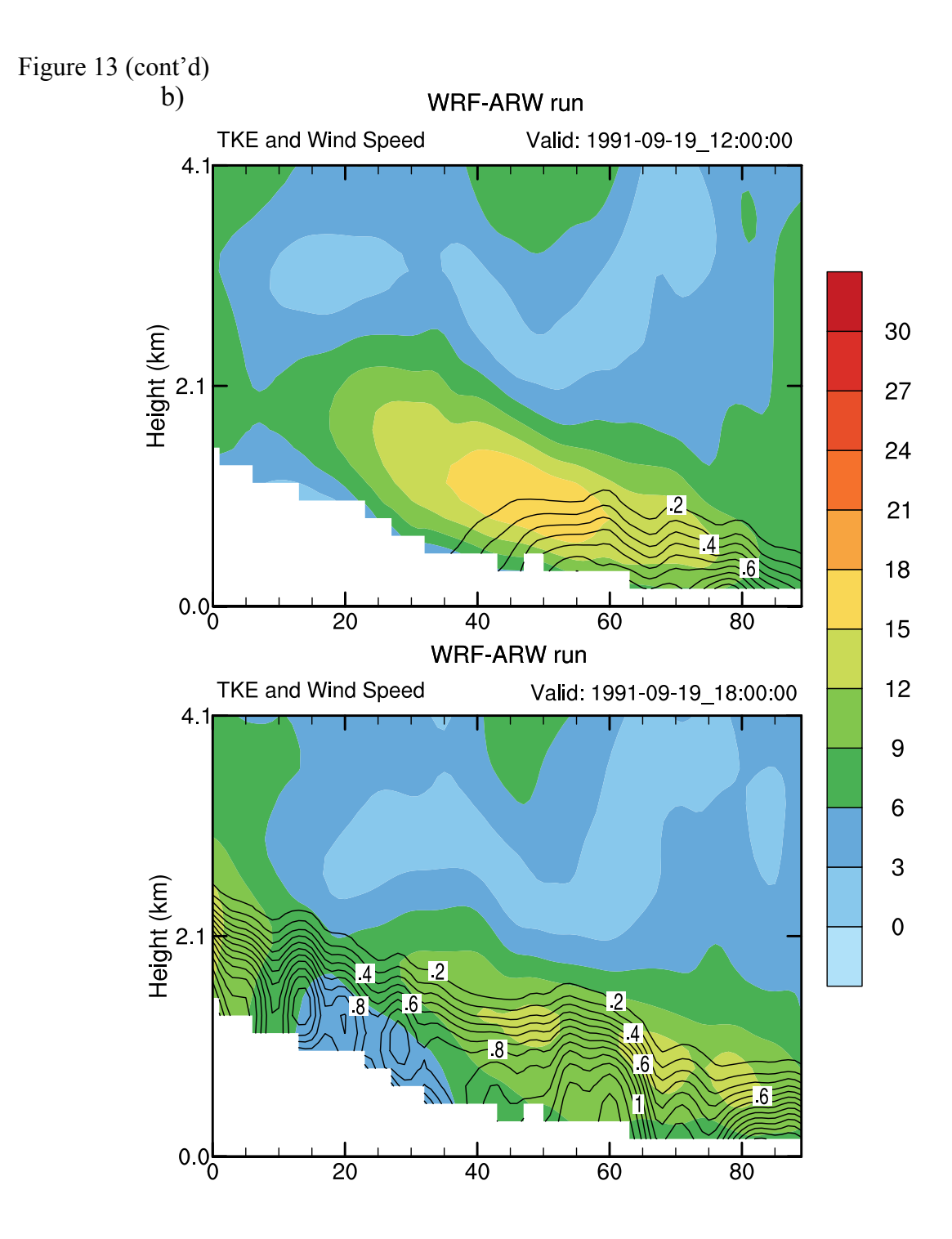


Figure 13. Same as Figure 7, but for September 19, 1991 with the center of the cross sections near the OUN station.



The core of the NLLJ (maximum wind speed exceeding 15 ms⁻¹) expanded over a large distance in the horizontal direction and somewhat smaller distance in the vertical direction. The height of the jet core appears to be following the terrain, with perhaps a slight tilt upward with

increasing terrain elevation towards west. In the early morning (12 UTC), the lower atmosphere is characterized by an inversion and the jet core appears to be above the surface-based inversion. At noon (18 UTC), a mixed layer has grown to more than 1000 m, which again appears to be following the terrain. The jet core is above the mixed layer in the elevated inversion layer. The strength of the jet is reduced at 18 UTC compared to 12 UTC, which may be due to a combination of the reduced horizontal temperature gradient by more intense daytime turbulent mixing and the moving of the jet core downstream.

More detailed effect of the NLLJ on the temperature and moisture fields is examined in Figure 14 which shows wind vector, potential temperature, and specific humidity at the maximum jet level. Unlike the southerly LLJ that is responsible for transporting warm, moist air from the Gulf of Mexico to the Great Plains, the NLLJ appears to transport dry, cool air from the northern plains southward. Initially there exists a sharp north-south gradient in both temperature and moisture fields. The specific humidity in the north is less than 4 g kg⁻¹ and it is more than 12 g kg⁻¹ in the south. The potential temperature is 292 K in the north, increasing to 304 in the south. The strongest gradient is initially located in the middle of the region, and with the intensification of the NLLJ, the front is pushed farther to the south-southeast. By the end of the period, the cold, dry air prevails over most of the region except for near the southern boundary.

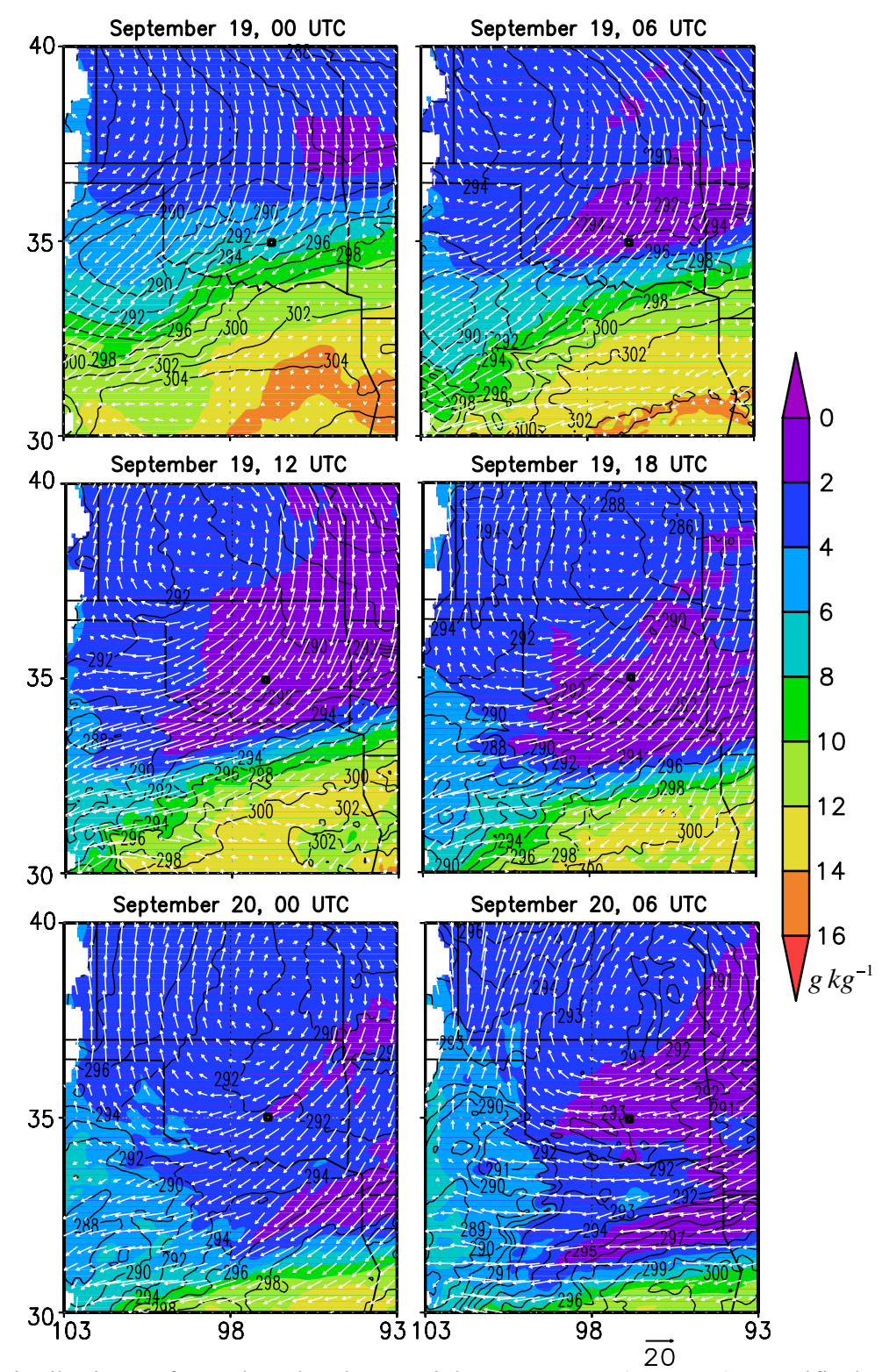


Figure 14. Distributions of 875 hPa level potential temperature (contours), specific humidity (shading) and wind vectors for the time period between 00 UTC, 19 September and 06 UTC, 20 September, 1991.

The time variation of vertical wind profiles are shown in Figure 15 from the model grid point nearest to OUN for the anticyclone case. Also shown in Fig. 15 are potential temperature and specific humidity profiles. In the September case, the jet profile first appears at 00 UTC on 19 Sept. The maximum wind speed gradually increases from 12 ms⁻¹ to just below 16 ms⁻¹ by 12 UTC the next morning, and finally reaches the maximum speed of 17 ms⁻¹ at noon (18 UTC) before starting to dissipate. There is considerable drying accompanying the development of the NLLJ especially above 900 hPa.

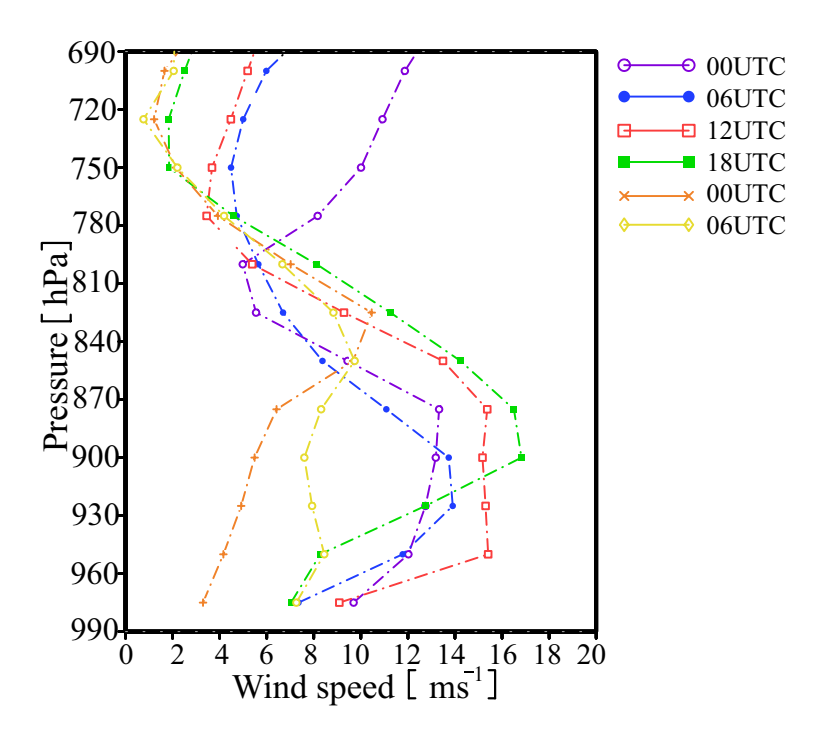
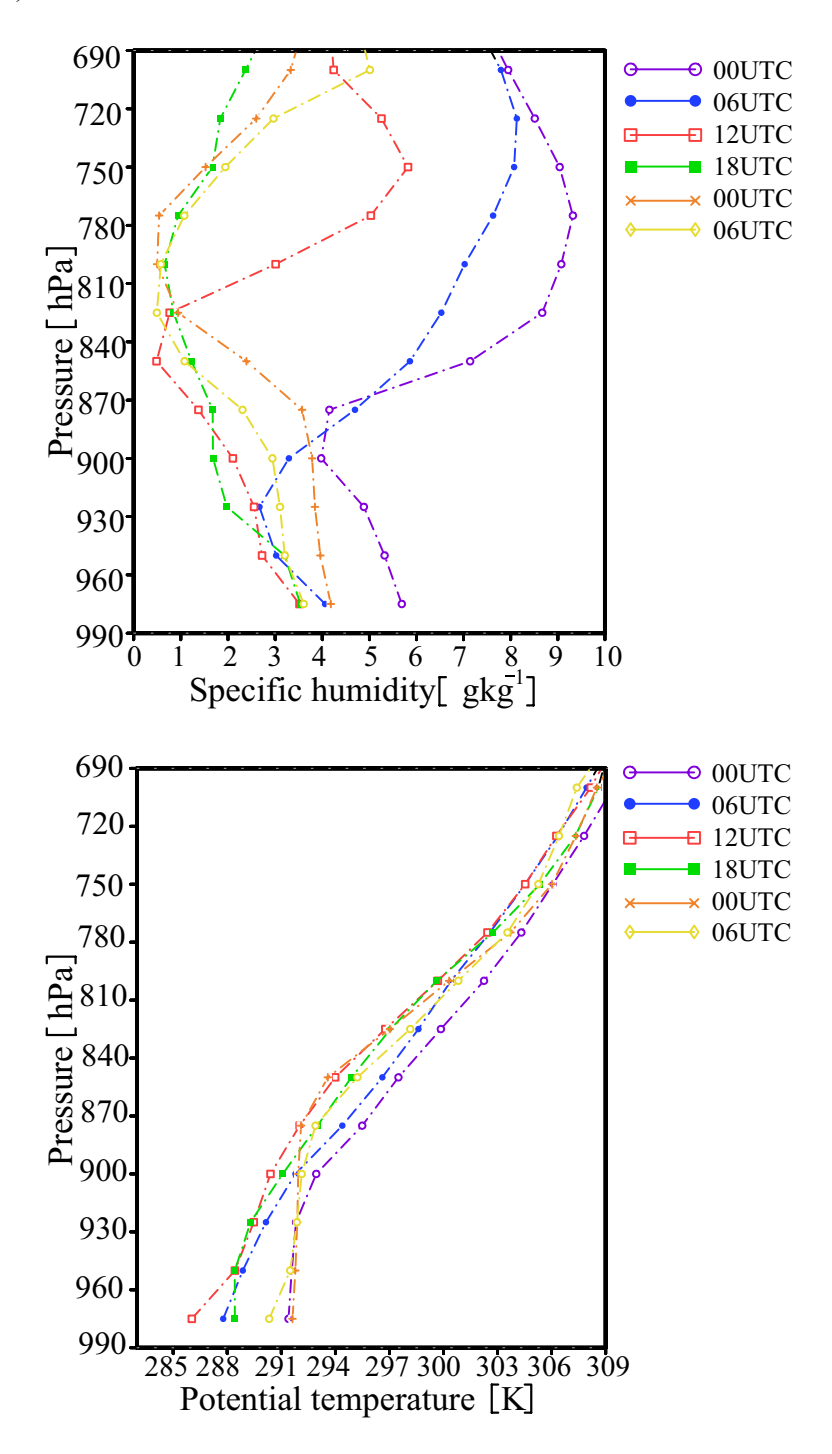


Figure 15. Vertical profiles of simulated wind speed, specific humidity and potential temperature at OUN station on 19 September, 1991.

Figure 15 (cont'd)



The results above suggest that twice daily temporal resolution of the rawinsonde sounding observations is too coarse to properly capture the time variation of the NLLJs. Remote

sensing techniques, such as radar wind profilers that give hourly profiles, would provide necessary resolution for study the NLLJ phenomenon.

CHAPTER VI

Discussion

Two cases of northerly LLJ over the Great Plains are picked for this study. The first case occurred on April 29, 1991, and the jet is associated with a strong surface low. The jet is located at the west side of the cyclone, below the upper-level jet. The main characteristics of the synoptic conditions accompanying this case are the change of the tilt in the low's axis. From 12 UTC on April 28 to 12 UTC on April 29, the upper-level trough changed its orientation from northeastsouthwest to northwest-southeast, indication that the surface cyclone is in its deepening stage. The wind is northerly, bringing cold and dry air from Canada as far south as Kansas and Missouri. The NLLJ on the west side of the surface cyclone was from the north, while at the upper levels winds were from the south. Similar to the anticyclone case in September, the jet is located at the top of mixing layer, but the stronger wind shear in the cyclone case produced stronger turbulent mixing (as indicated by larger values of TKE), placing the jet higher above the ground compared to the anticyclone case. East-west oriented cross sections also revealed that over 6-hour period (from 12 UTC to 18 UTC on April 29), the westward tilt of the cyclone axis increased, causing sinking of the cold air close to the surface and therefore increasing surface temperature gradient. All these factors contributed to further intensification of the jet.

The jet associated with an anticyclone synoptic system occurred on 19 September, 1991. The jet is located at the southeast side of the High, with winds predominantly coming from the northeast. An examination of the time evolution of the pressure, temperature, and wind fields revealed the synoptic conditions and the variation for the jet case. Strengthening of the High

rotates cold and dry air southward, creating temperature gradient over northern Texas, Oklahoma, and south Kansas. As a result of this gradient, winds accelerated and at 12 UTC on September 19, a LLJ developed at the elevation of approximately 1000 m above the ground. The LLJ is located further south from the upper-level jet, in the area of the minimum vorticity. The role of the boundary layer plays in the jet formation is investigated by looking at the vertical cross sections on the plan perpendicular to the jet core. It is evident that the jet is located at the top of the PBL where the horizontal temperature gradient is the strongest. As the boundary layer grew higher during the day, so did the elevation of the jet core. The horizontal extension of the jet core is significantly bigger than the vertical extension, and because of an increase in the PBL depth and the jet elevation, vertical extension of the jet decreases even more over daytime. A sharp increase in the TKE values is located just below the jet at 12 UTC indicating that the jet characteristics might have influence on the PBL characteristics [as implied by Charney et al. (2003) in their wildfire analysis]. Six hours later, with increased PBL depth and decreased temperature gradient, the jet core elevates following the growth of in the PBL height.

An analysis of temperature and moisture fields confirmed that in both September and April cases, cold and very dry air originating from Canada is advected southward. In the case of anticylonic flow, dry air is transported by a LLJ from northeast to southwest, but as the jet losses its strength, temperature and moisture gradient are pushed further to the east and south with the clockwise rotation over the surface High. On the other hand, in the April case, very cold and dry air is transported northward by the cyclonic rotation, and then quickly moved eastward with the same cyclonic circulation. The same characteristics of a cyclonically turning branch of a dry air stream associated with a mid-latitude cyclone are noted in a study by Carlson (1980). Because of different dynamics of the two synoptic features, in the anticyclone case, dry and cold air

transported by the NLLJ is extended over a larger area than the air transported by the jet in the cyclone case. Advection of cold and dry air by a low-level jet could have a significant impact on the development of severe weather conditions such as winter blizzards, and may favor the development of fuels for wildfires.

Despite the differences in turbulence mixing and boundary layer structure between the two cases, the peak wind or the jet nose were positioned in the elevated inversion layer just above the boundary layer, where the temperature gradient is strongest. Below the jet nose, wind speed decreases due to a decrease in temperature gradient as a result of mixing in the PBL, while above the jet nose, gradual decrease in wind speeds can be explained again by a decrease of temperature and pressure gradient with height. Also, as the boundary layer grew higher during the day, so did the elevation of the jet core. The fact that the jet occurs above the daytime boundary layer suggests that these northerly LLJs are not impacted by the boundary layer characteristics and the mechanisms that are believed to be a major cause for the southerly LLJ over the Great Plains or other nocturnal LLJs. In both cases, the northerly low-level jet is forced primarily by synoptic-scale pressure and temperature gradients. Figure 16 confirms these claims, showingstrong geostrophic and ageostophic winds located where the jet is located both in the cyclonic and anticyclonic cases. In a jet located on the southern side of the anticyclone, the wind speeds are lower due to weaker pressure gradient compared to the jet in the cyclonic flowcase.

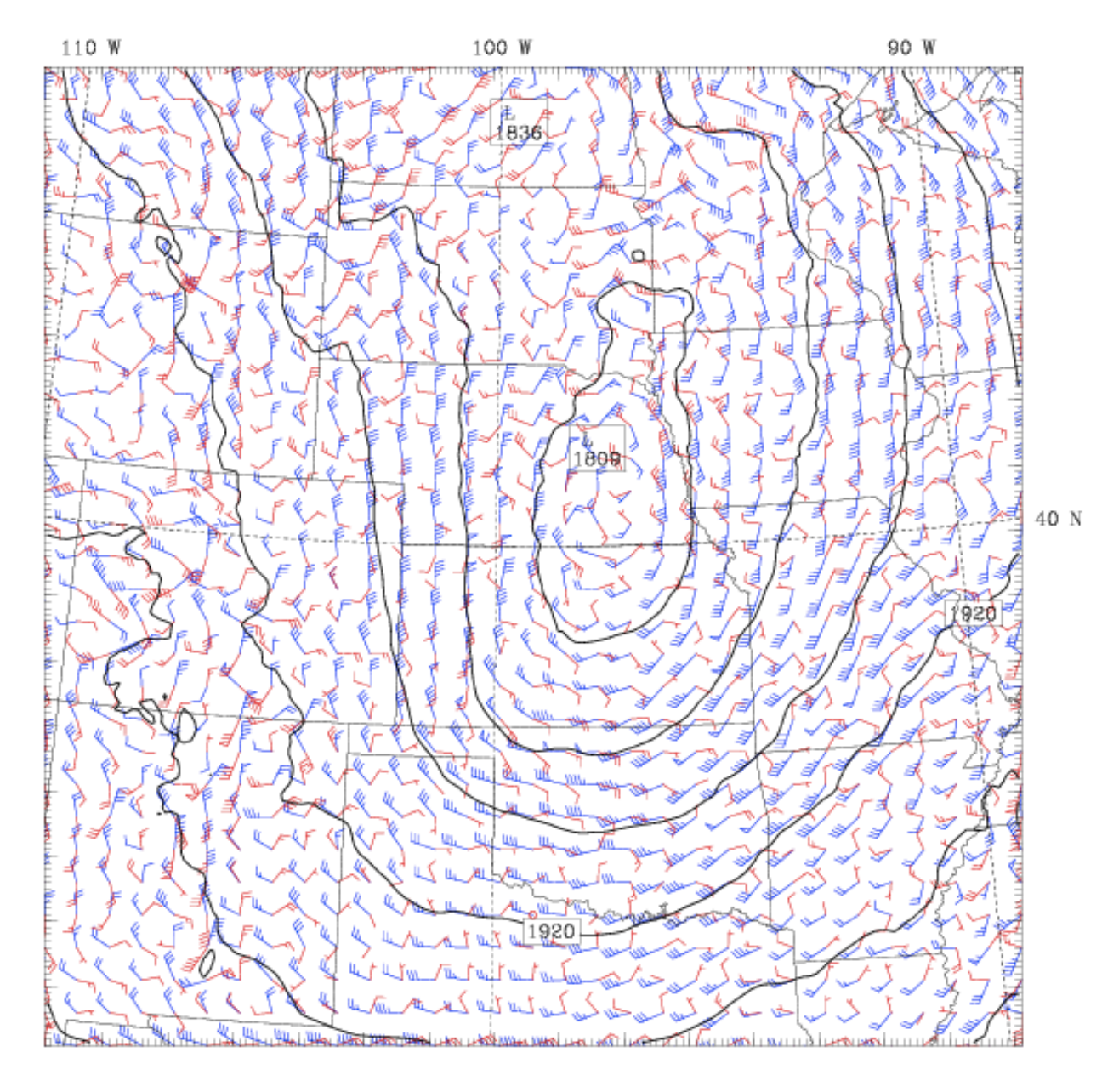
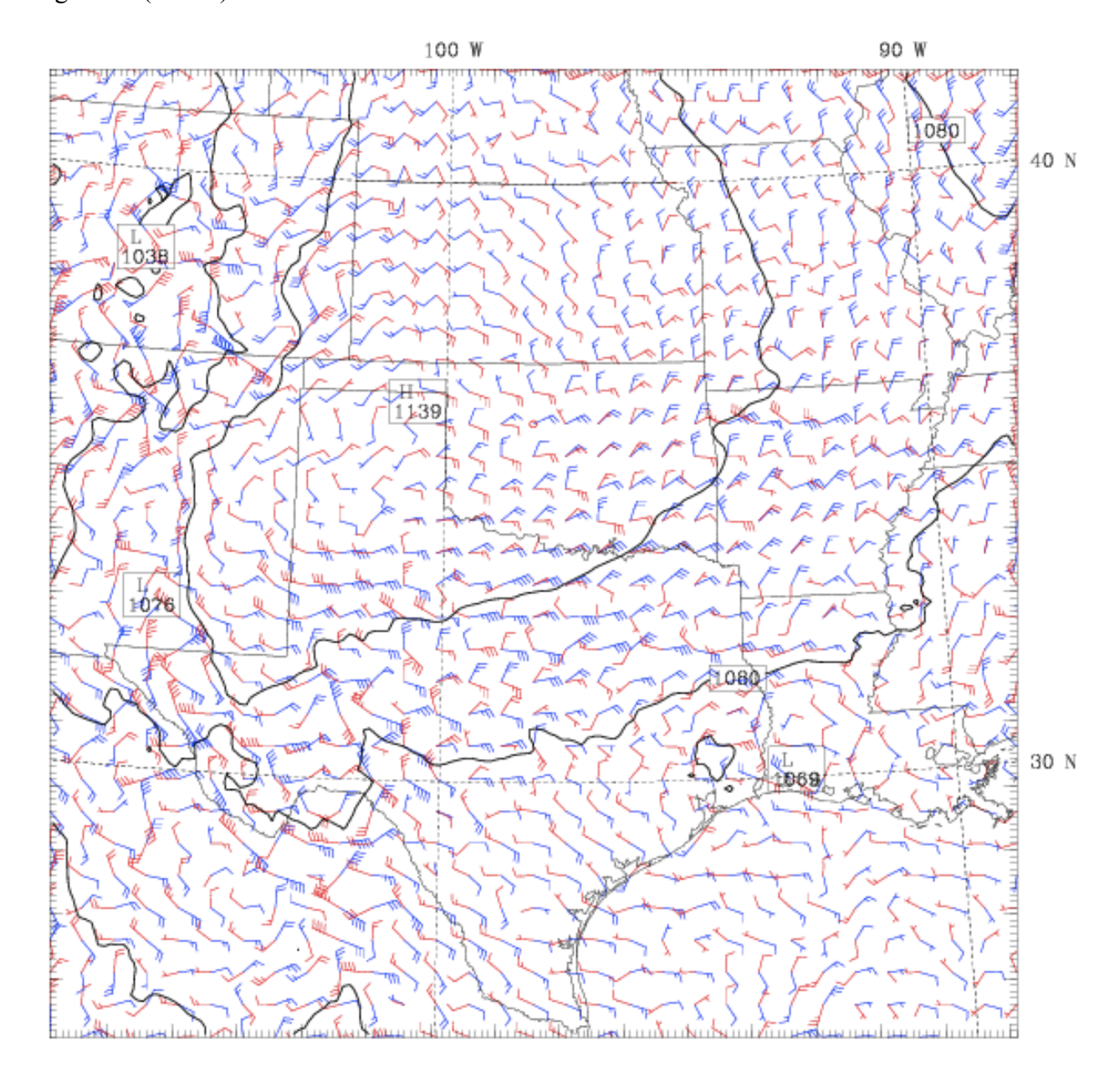


Figure 16. Geostrophic (blue) and ageostrophic (red) wind at 800 hPa surface on April 29, at 12 UTC (upper), and at 900 hPa surface on September 19, at 12 UTC (bottom).

Figure 16 (cont'd)



All our findings are in agreement with findings of previous studies of synoptic-scale LLJs (Sladkovic and Kanter1976; Charney et al. 2003; Walters et al. 2008). These jets are forced by a various synoptic-scale features. Compared to other jet types, this jet type has stronger maximum wind speed, with the jet core located at the base of the elevated inversion layer just above the planetary boundary layer.

CHAPTER VII

Summary and Conclusion

In this study, the WRF model was used to simulate two episodes of northerly low-level jet in central U.S. with the purposes of assessing the model's ability in capturing these northerly jets and better understanding their structure and impacts and the large-scale environment from which they form.

The two jet episodes were chosen for the study because they were associated with completely different synoptic pressure systems, with the spring jet case accompanied by a strong mature cyclone, and the fall jet case associated with a broad anticyclone. As noted by Walter and Winkler (personal communication), approximately 52% of the jet events they analyzed were related anticyclones, while 37% with cyclonic airflows. The WRF model was quite successful in simulating the strengths and positions of the High/Low and the associated pressure and temperature gradients in the two cases. The maximum observed wind speed (28 ms⁻¹) and the height where the maximum appeared (790 hPa level) were significantly higher in the spring jet case than the fall jet case (20 ms⁻¹ at 888 hPa level). The model skillfully captured the differences in the strength and elevation of the jets between the two cases. The height of the jet nose was simulated well, but the maximum wind speed was underestimated by 20-25%. The wind speed minimum above the jet nose and the elevation at which it occurred were in good agreement with the observations which, when combined with the weaker wind maximum, led to weaker wind shear in the simulation compared to the observation. In both cases, the wind direction shift with height was captured very well by the model.

The model result confirmed that the spring jet reached its maximum strength early in the morning around 12 UTC, while the fall jet reached its maximum strength later in the day at approximately 18 UTC, which was missed by the twice daily observations. The model results suggested that the core of the northerly low-level jet was almost 450 km wide and 800 m deep on a west-east cross section in the fall case, while it was approximately 250 km wide and 1200 m deep in the spring case.

Despite the differences in the vertical structure of the jet profile between the two cases, the jet nose or the peak wind was located in the stable air at the top of the boundary layer in both cases. As the boundary-layer height grow from a few hundred meters in early morning to more than 1 or 2 km in the afternoon in response to the surface heating and the intensification of turbulence mixing in the boundary layer, the height of the jet nose was also lifted to higher level. This feature, together with the result that the simulated jet was not sensitive to boundary layer and land surface schemes used by the model, suggested that these northerly jets were not forced primarily by boundary layer processes such as the inertial oscillation as in many of the southerly jet cases that occur at night. Instead, these northerly jets were part of large-scale flows that typically develop on the east and southeast side of an anticyclone and on the west and southwest side of a cyclone where the strong pressure gradient was found.

Unlike the southerly low-level jets that play a significant role in transport warm, moist air from Gulf of Mexico over to the Great Plains, the northerly low-level jet is responsible for advection of colder and dryer air from Canada southward. Air transported from north by clockwise-rotating anticyclone is almost 50% dryer than air that is advected in the area from south, south-east by a clockwise-rotating cyclone. While southerly low-level jet was often associated with nocturnal convective storms, these northerly jets are often associated with severe

weather condition (in the case of cyclone) and with conditions prone to the development and easier spread of a forest fires (in the case of the anticyclone).

As mentioned above, NLLJ is responsible for advection of cold and dry air from Canada, and that dry and cold air is significant factor in development of winter storms. Charney et al. (2003) were looking at the Mack Lake fire and used the MM5 model simulation to look at interaction between LLJ and the fire. Previous analyses of the Macs Lake fire case found that main contributor to the fire spreading were high surface winds and low relative humidity of the air. Charney et al. (2003) proposed development of an index that would emphasize places where interaction between mixed layer and LLJ occur, in order to predict places where kinetic energy and TKE associated with the jet can encourage further development of an existing or early developing forest fire. Also, northerly low-level jet because of its advection of cold and dry air has a great impact on agriculture. Therefore, better understanding of the jet physics and dynamic characteristics and forecasting of the jet is necessary in order to prevent potentially great financial losses.

Future comprehensive study of the NLLJ is necessary. In order to better explain and investigate this phenomenon, surface observations with better spatial and temporal resolution are critical component, next to high resolution measurements of vertical profiles of temperature, moisture and wind. As suggested by Walters et al. (2008), widely available reanalysis data should be carefully used in climatological studies of the low-level wind maximum, and without appropriate evaluation and comparison with the observations they may lead to false conclusions. This study examined only two cases; more cases are needed in order to properly evaluate and explain all possible mechanisms involved in the NLLJ initialization and development.

APPENDIX

APPENDIX

WRF ARW has wide selection of physical and dynamical options available. Choice of specific parameterization scheme in the model can have a major impact on the results of the model simulation.

More detailed list of all available physics and dynamics options in the WRF version 3 can be found at the Mesoscale and Microscale Meteorology (MMM) Division of the NCAR Earth System Laboratory (NESL) web page:

http://www.mmm.ucar.edu/wrf/users/docs/user guide V3/contents.html

This section offers more details on the specific options we used in our simulations (Table 1).

Microphysics (mp physics)

Microphysics explicitly resolves water vapor processes, as well as cloud and precipitation processes. Option we used in our runs are:

- WRF Single-Moment 5-class scheme: WSM5 scheme treating vapor, rain, snow, cloud
 ice, and cloud water, and allows supercooled water to exist, as well as gradual melting of
 snow below the melting layer. Suitable for mesoscale integrations.
- WRF Single-Moment 6-class scheme: The WSM6 scheme on all above mentioned for WSM5 includes graupel and its associated processes. Suitable for high-resolution

simulations.

Cumulus Parameterization (cu physics)

Cumulus parameterization schemes are responsible for treating effects of sub-grid convection and shallow clouds, fluxes related to updrafts and downdrafts and compensation motion outside the clouds. Also, gives the convective component of total surface precipitation. Options we used:

- Kain-Fritsch scheme: Kain-Fritch scheme is a simple cloud model, that treats deep and shallow convection, with updraft and downdraft of moist.
- Betts-Miller-Janjic scheme. Operational Eta scheme: Betts-Miller-Janjic scheme looks at deep and shallow convection as a function of entropy change.

Land Surface (sf surface physics)

The land-surface model combines information from the surface layer scheme, radiative forcing, precipitation forcing from microphysics scheme, and convective scheme, together with land-surface properties, to calculate heat and moisture flux over land and sea-ice grid points. These fluxes are used in PBL scheme as lower boundary conditions for vertical mixing.

- 5-layer thermal diffusion: scheme is based on the MM5 5-layer soil temperature model, with 1, 2, 4, 8, and 16 cm thick layers. Below these layers, the temperature is fixed at a deep-layer average. The energy budget includes radiation, sensible, and latent heat flux
- Noah Land Surface Model: Noah land-surface model is a 4-layer soil temperature and moisture model. The layer thicknesses are 10, 30, 60 and 100 cm (adding to 2 meters)

from the top down. The scheme provides sensible and latent heat fluxes to the boundary-layer scheme.

 Pleim-Xiu Land Surface Model: the PX land-surface model includes a 2-layer soil temperature and moisture model, with first layer 1 cm thick, and the lower layer 99 cm tick.

Surface Layer (sf sfclay physics)

The surface layer schemes provide stability-dependent information about the surface for the land-surface and PBL scheme.

- Eta similarity: 8 runs have used the Eta surface layer scheme, based on Monin-Obukhov similarity theory. The scheme includes parameterization of a viscous sub-layer. All surface fluxes are computed by an iterative method.
- Pleim-Xiu surface layer: 9th run have used the PX surface layer scheme and it's based on similarity theory and includes a viscose sub-layer in the form of quasi-laminar boundary layer.

Planetary Boundary layer (bl pbl physics)

The planetary boundary layer (PBL) is responsible for vertical sub-grid-scale fluxes due to eddy transports. The PBL schemes determine the flux profiles within the well-mixed boundary layer and the stable layer, and thus provide atmospheric tendencies of temperature, moisture (including clouds), and horizontal momentum in the entire atmospheric column.

Mellor-Yamada-Janjic Level 2.5 PBL (5). PBL Mellor-Yamada Janjic TKE parameterization of turbulence in the PBL and in the free atmosphere represents an implementation of the Mellor-Yamada Level 2.5 turbulence closure model through the full range of atmospheric turbulent regimes. In this implementation, an upper limit is imposed on the master length scale.

ACM2 PBL

BouLac PBL : Bougeault-Lacarrère PBL.

Longwave Radiation (ra lw physics) and Shortwave Radiation (ra sw physics)

The radiation schemes provide atmospheric heating due to radiative flux divergence and surface downward longwave (thermal radiation absorbed and emitted by gases and surfaces) and shortwave radiation (visible and surrounding wavelengths that make up the solar spectrum) for the ground heat budget. The processes include absorption, reflection, and scattering in the atmosphere and at surfaces. For shortwave radiation, the upward flux is the reflection due to surface albedo.

CAM scheme: Radiation is CAM longwave, as used in the NCAR Community
 Atmosphere Model (CAM 3.0) for climate simulations. It interacts with resolved clouds
 and cloud fractions.

Shortwave radiation is also CAM. It has the ability to handle optical properties of several aerosol types and trace gases. It uses cloud fractions and overlap assumptions in unsaturated regions, and has a monthly zonal ozone climatology.

REFERENCES

REFERENCES

Augustine, J. A., and F. Caracena. 1994: Lower-tropospheric precursors to nocturnal MCS development over the central United States. Weather and Forecasting, **9**, 116–35.

Buzzi, A., and L. Foschini, 1999: Mesoscale meteorological features associated with heavy precipitation in the southern Alpine region. Meteorol. Atmos. Phys, **72**,131-146.

Bonner, W.D., 1968: Climatology of the low-level jet. Mon. Wea. Rev., 96, 833-850.

Brook, R. R., 1985: The Koorin nocturnal low-level jet. Boundary-Layer Meteorology, **32**, 133-154.

Carlson, T. N., 1980: Airflow through midlatitude cyclones and the comma cloud pattern. Mon. Wea. Rev., **108**, 1498-1509.

Charney, J. J., X. Bian, B. E. Potter, and W. E. Heilman 2003: Low level jet impact on fire evolution in the Mack Lake and other severe wildfires. 2d International wildland fire ecology and Fire Management Congress: 5th symposium of Fire and forest meteorology; American Meteorological Society.

Collins, W.D., P. J. Rasch, B. A. Boville, J. J. Hack, J. R. McCaa, D. L. Wiliamson, J. T. Kiehl, B. Briegleb, C. Bitz, S. Lin, M. Zhang, and Y. Dai, 2004: Description of the NCAR Community Atmosphere Model (CAM 3.0). NCAR Technical Note, NCAR/TN-464+STR, 226pp.

Cross, P. S., 2003: The California Costal Jet: Synoptic Controls and Topographically Induced Mesoscale Structure. Ph.D. dissertation.

Drobinski, P., S. Bastin, V. Guenard, J.-L. Caccia, A.M. Dabas, P. Delville, A. Protat, O. Reitebuch, and C. Werner, 2005: Summer mistral at the exit of the Rhône valley. Q.J.R. Meteorol. Soc., 605, 352-375.

Findlater, J., 1969: A major low-level air current near the Indian Ocean during the northern summer.Quart. J. R. Met. Soc., 95, 361-380.

Frisch, A. S., B. W. Orr, and B. E. Martner, 1992: Doppler radar observations of the development of a boundary-layer nocturnal jet. Monthly Weather Review, **120**, 3–16.

Jury, M. and G. Spencer-Smith, 1988: Doppler sounder observations of trade winds and sea breezes along the African west coast near 34 ° S, 19 ° E. Boundary Layer Meteorology, **44**,373-405.

Jury, M. R. and G. R. Tosen, 1989:Characteristics of the winter boundary layer over the African Plateau: 26 ° S. Boundary-Layer Meteorology, **49**, 53-76.

Kapela, A. F., P. W. Leftwich, and R. Van Ess, 1995: Forecasting the impacts of strong wintertime post-cold frontal winds in the Northern Plains. Wea. Forecasting, **10**, 229-244.

Kelbe, B. 1988: Features of westerly waves propagating over southern Africa during summer. Monthly Weather Review, **116**, 60-70.

LaBar, R. J., 2006: The Llanos Low-Level Jet and its Association with Venezuelan Convective Precipitation. National Weather Center Research Experiences for Undergraduates, Central Washington University, Ellensburg, WA (final project)

Lebeaupin Brossier, C. and P. Drobinski, 2009: Numerical high-resolution air-sea coupling over the Gulf of Lions during two tramontane/mistral events. J. Geophys. Res., **114**, D10110, doi:10.1029/2008JD011601.

Lebeaupin, C., V. Ducrocq, and H. Giordani, 2006: Sensitivity of Mediterranean torrential rain events to the sea surface temperature based on high-resolution numerical forecasts, J. Geophys. Res., 111, D12110,doi:10.1029/2005JD006541.

McCorcle, M. D., 1988: Simulation of surface-moisture effects on the Great Plains low-level jet. Monthly Weather Review, **116**, 1705-1720.

Membery, D. A., 1983: Low-level wind profiles during the Gulf Shamal. Weather, 38, 18-24.

Mesinger, F., G. Dimego, E. Kalnay, K. Mitchell, P. C. Shafran, W. Ebisuzaki, D. Jović, J. Woollen, E. Rogers, E. H. Berbery, M. B. Ek, Y. Fan, R. Grumbine, W. Higgins, H. Li, Y. Lin,

G. Manikin, D. Parrish, and W. Shi, 2006: North American Regional Reanalysis. Bulletin of the American Meteorlogical Society, **87**, 343–360.

Paegle, J., and D. W. McLawhorn, 1983: Numerical modeling of diurnal convergence oscillations above sloping terrain. Monthly Weather Review, 111, 67–85.

Pal, J.S., F. Girogi, X. Bi, N. Elguindi, F. Solmon, X. Gao, S.A. Rauscher, R. Francisco, A. Zakey, J. Winter, M. Ashfaq, F.S. Syed, J.L. Bell, N.S. Diffenbaugh, J. Karmacharya, A. Konare, D. Martinez, R.P. da Rocha, L.C. Sloan, and A.L. Steiner, 2007: Regional climate modeling for the developing world: The ICTP RegCM3 and RegCNET. Bull. Amer. Meteorol. Soc., 88, 1395-1409.

Parish, T., 2000: Forcing of the summertime low-level jet along the California coast. Journal of Applied Meteorology, **39**, 2421-2433.

Parish, T. R., A. R. Rodi, and R. D. Clark, 1988: A case study of the summertime Great Plains low level jet. Monthly Weather Review, **116**, 94–105.

Pielke, R.A., W.R. Cotton, R.L. Walko, C.J. Tremback, W.A. Lyons, L.D. Grasso, M.E. Nicholls, M.D. Moran, D.A. Wesley, T.J. Lee, and J.H. Copeland, 1992: A comprehensive meteorological modeling system -- RAMS. Meteor. Atmos. Phys., **49**, 69-91.

Pitchford, K. L., and J. London, 1962: The low-level jet as related to nocturnal thunderstorms over Midwest United States. Journal of Applied Meteorology, **1**, 43–47.

Sénési, S., P. Bougeault, J. Chèze, P. Cosentino, and R. Thepenier, 1996: The Vaison-La-Romaine Flash Flood: Mesoscale Analysis and Predictability Issues. Wea. Forecasting, **11**, 417–442.

Skamarock, W. C., J. B. Klemp, J. Dudhia, D. O. Gill, D. M. Barker, W. Wang, and J. G. Powers, 2008: A description of the Advanced Research WRF Version 3. NCAR Tech Notes.

Sládkovič, R. and H. -J. Kanter, 1976: Low-level jet in the Bavarian pre-alpine region. Meteorology and Atmospheric Physics, **25**, 343-355.

Saulo, A. C., M. Nicolini, and S. C. Chou, 2000: Model characterization of the South American

low-level flow during the 1997-1998 spring-summer season. Climate Dyn., 16, 867–881.

Silva, M. C. Lemos, R. P. Rocha, and R. Y. Ynoue, 2010: Climatic simulations of the eastern Andes low-level jet and its dependency on convective parameterizations. Meteorology and Atmospheric Physics, 108, 9-27.

Sijikumar, S. 2003: Low Level Jet stream of Asian Summer Monsoon and its variability. Ph.D. dissertation, Department of Atmospheric Science, Cochin University of Science and Technology.

Song, J, K. Liao, R. L. Coulter, and B. M. Lesht, 2003: Climatology of the low-level jet at the southern Great Plains atmospheric Boundary Layer Experiments site. Journal of Applied Meteorology, 44, 1593-1606.

Storm B., J. Dudhia, S. Basu, A. Swift, I. Giammanco, 2008: Evaluation of the Weather Research and Forecasting Model on Forecasting Low-level Jets: Implications for Wind Energy, Wiley Interscience, **12**, 81–90.

Vernekar, A., B. Kirtman, and M. Fennessy, 2003: Low-level jets and their effects on the South American summer climate as simulated by the NCEP Eta Model. J. Climate, **16**, 297–311.

Walters, C. K., and J. A. Winkler, 2001: Airflow configurations of warm season southerly low-level wind maxima in the Great Plains: Part I. Spatial and temporal characteristics and relationship to convection. Weather and. Forecasting, **16**, 513–30.

Walters, C., K, 2001: Airflow configurations of warm season southerly low-level wind maxima in the Great Plains. Part II: The synoptic and subsynoptic-scale environment. Wea. Forecasting, **16**, 531-551.

Walters, C. K., J. A. Winkler, R. P. Shadbolt, J. van Ravensway, and G. D. Bierly, 2008: A Long-Term Climatology of Southerly and Northerly Low-Level Jets for the Central United States, Annals of the Association of American Geographers, 98, 521-552.

Whiteman, C. D., X. Bian, and S. Zhong. 1997. Low-level jet climatology from enhanced rawinsonde observations at a site in the southern Great Plains. Journal of Applied Meteorology, **36**, 1363–76.

Zhong, S., J. D. Fast, and X. Bian, 1996: A case study of the Great Plains low-level jet using wind profiler network data and a highresolution mesoscale model. Monthly Weather Review, 124, 785–806.

Zhong, Z. and H. Wang, 2000: A study of the relationship between low-level jet and inversion layer over an agroforest ecosystem in east china plain. Advances in Atmospheric Sciences, 17, 299-310.